SIAM J. Applied Dynamical Systems
Vol. 14, No. 4, pp. 2030–2068

Tipping Points Near a Delayed Saddle Node Bifurcation with Periodic Forcing*

Jielin Zhu†, Rachel Kuske†, and Thomas Erneux‡

Abstract. We consider the effect on tipping from an additive periodic forcing in a canonical model with a saddle node bifurcation and a slowly varying bifurcation parameter. Here tipping refers to the dramatic change in dynamical behavior characterized by a rapid transition away from a previously attracting state. In the absence of the periodic forcing, it is well known that a slowly varying bifurcation parameter produces a delay in this transition, beyond the bifurcation point for the static case. Using a multiple scales analysis, we consider the effect of amplitude and frequency of the periodic forcing relative to the drifting rate of the slowly varying bifurcation parameter. We show that a high frequency oscillation drives an earlier tipping when the bifurcation parameter varies more slowly, with the advance of the tipping point proportional to the square of the ratio of amplitude to frequency. In the low frequency case the position of the tipping point is affected by the frequency, amplitude, and phase of the oscillation. The results are based on an analysis of the local concavity of the trajectory, used for low frequencies both of the same order as the drifting rate of the bifurcation parameter and for low frequencies larger than the drifting rate. The tipping point location is advanced with increased amplitude of the periodic forcing, with critical amplitudes where there are jumps in the location, yielding significant advances in the tipping point. We demonstrate the analysis for two applications with saddle node–type bifurcations.

Key words. tipping points, multiple scales, delayed bifurcation, periodic forcing, asymptotic expansions

AMS subject classifications. 34E13, 37B55, 35B32, 37L10, 34E10

DOI. 10.1137/140992229

1. Introduction.

Generally speaking, the term tipping point refers to an abrupt transition in dynamical behavior observed as the system moves to a qualitatively different state, due to small changes in one or more factors [1]. Tipping points have been observed in many different fields, including the start and end of ice ages [2], environmental regime shift [3], synchronized behavior of neural activity [4], catastrophic collapse in ecology, and power systems [5]. As many of these transitions are often irreversible or difficult to reverse, it becomes important to develop analytical techniques for predicting the location of tipping points and understanding the key contributing factors to tipping.

A number of analyses indicate that tipping points can depend on the bifurcation structure of the system, external noise or forcing, or the drifting rate of parameters that vary in time

*Received by the editors October 20, 2014; accepted for publication (in revised form) by J. Sieber August 31, 2015; published electronically November 24, 2015.
http://www.siam.org/journals/siads/14-4/99222.html

†Department of Mathematics, University of British Columbia, Vancouver, BC V6T 1Z2, Canada (jielinzhu@math.ubc.ca, rachel@math.ubc.ca). The work of the first and second authors was supported in part by a Natural Sciences and Engineering Research Council Discovery Grant.

‡Optique Nonlineaire Theorique, Universite Libre de Bruxelles, B-1050 Brussels, Belgium (terneux@ulb.ac.be). The work of this author was supported in part by Distinguished Visitor Grants at the Pacific Institute of Mathematical Sciences and the Peter Wall Institute for Advanced Studies. This author also acknowledges the support of the F.N.R.S. (Belgium).

[6]. Of course, in applications a combination of these factors may contribute to the system simultaneously. A significant number of studies have focused on systems that have a slowly varying parameter approaching a saddle node bifurcation point, where the transition occurs for parameter values beyond that of the static bifurcation point, known as a delayed bifurcation. Earlier recognition of this phenomenon is discussed in the context of optics [7] and neuronal dynamics [8], as well as general bifurcation theory [9]. The structure appears in many applications, including models of global energy balance [10], extent of Arctic sea ice [11, 12], and population resilience [5], to name a few. Focal points for prediction of tipping include statistical measures based on historical data that track the value of the slowly varying parameter where an abrupt transition occurs [14]. These types of measures have been compared with canonical models, illustrating that in the presence of noise tipping can occur well before the slowly varying parameter reaches the static bifurcation point of the model [15]. Whether the location of the tipping point is advanced, that is, "early," or delayed relative to the static bifurcation point depends on the relationship between the drifting rate and the strength of the noise, as studied for different underlying bifurcation structures in [16, 18]. Predictive techniques using statistical measures and time series analyses have been developed to identify signatures of proximity to a tipping point or potential for early tipping, with examples in [3, 5, 14, 19] and additional references in [20]. However, those measures are not necessarily applicable if the tipping is driven by changes in the drifting rate or other factors, indicating that a better understanding of the role of different tipping mechanisms is necessary.

An additional factor appearing in many applications is periodic variation. Often reduced models, such as those for the extent of Arctic sea ice [11, 12, 13], are developed for analysis by averaging over oscillations with higher frequency, but a closer look at these types of models indicates different locations of the tipping points when the oscillations are included. Periodic variation can occur on different time scales, such as the seasonal variation considered in [11] or regular fluctuations on the time scale of decades [21]. To explore the effect of periodic forcing with either low or high frequency, we consider the canonical model for a saddle node bifurcation with a slowly varying bifurcation parameter and additive periodic forcing. In this setting we explore how the location of the tipping point depends on the combined effect of frequency, amplitude, and the drifting rate at which the bifurcation parameter approaches the static bifurcation point. The different expansions that are necessary to cover the different scenarios provide explicit expressions for the tipping points and capture the key contributions that determine them.

For high frequency forcing, we use a multiple scales approach combined with layer expansions [22, 23, 24]. The outer expansion uses a multiple scales expansion based on the times scales of the oscillations and the drifting rate. The outer expansion does not provide the approximation for the tipping point, but indicates the location of the inner expansion composed of an oscillatory part plus a correction. Combining several multiple scales expansions in terms of fractional powers of the drifting rate to get the inner expansion, we find that the tipping point is determined from the averaged equation for the correction to the oscillatory contribution. The form of the averaged equation is similar to that of the case without oscillations, facilitating explicit expressions for two main contributions to the location of the tipping point relative to the static bifurcation point: a delay due to the slowly drifting bifurcation parameter, and an advance proportional to the square of the ratio of amplitude to frequency

for the oscillation. The shift due to high frequency periodic forcing is also compared with the case of white noise forcing. An additional rescaling is required in the case of both large amplitude and high frequency. That rescaling indicates that, in certain limits, the appropriate expansion for the rescaled system is the low frequency approximation rather than the high frequency case, as might be expected.

The multiple scales approach used for the high frequency oscillations is not applicable for low frequency oscillations. Rather, the oscillatory outer or regular solution can be written in terms of the slow time only, and where it does not exist, we find two different types of tipping points. For the first type, the outer solution vanishes but its derivative does not. Then a local approximation for the equation of the trajectory has a singularity corresponding to the tipping point. The influence of the oscillation appears through the derivative of the square of the outer solution. In contrast, for the second type of tipping point the derivative of the square of the outer solution also vanishes. Then a different local approximation is used to consider the concavity of the trajectory. The concavity indicates whether or not tipping occurs near this location. In contrast to the high frequency forcing, where the location of the tipping point varies smoothly with the other parameters, for parameter values where the concavity in the low frequency case changes there are discontinuities in the location of the tipping point. From the analysis of these two types of tipping points, we find that their location is affected not only by the frequency, the amplitude, and the drifting rate, but also by the behavior of the trajectory as the oscillations cause it to approach zero. This effect can be related to the phase of the oscillations, given by an initial condition, and can lead to either delayed or advanced tipping.

We demonstrate the method on two applications, namely, a Morris–Lecar model and an energy balance model describing the persistence of Arctic sea ice. In both cases, we use the approaches developed for the canonical model directly on normalized versions of these models. The analysis illustrates the importance of this normalization, as it is within the rescaled system that we can identify the relationships and approximations that lead to quantitative expressions for the tipping point. We also see that the results can be extended beyond the range of asymptotic relationships for drifting rate, frequency, and amplitude obtained in the context of the canonical model; for example, we consider the scenario where the ratio of amplitude to frequency is outside of these limits. The application of the approaches in these extended ranges is based on recognizing the leading order contributions in the outer and local expansions that provide information about the relevant features for tipping. These observations guide the inclusion of the most important terms in reduced equations with singularities corresponding to tipping points. Even without deriving these reduced equations, the normalized systems combined with the results from the canonical model already indicate parameter ranges where advanced tipping is predicted, as we discuss in the context of the specific applications.

In section 2, we introduce the canonical model with an additive periodic forcing. We briefly review the results when there is no oscillatory term. In section 3, we show that a high frequency oscillation changes the position of the bifurcation point for the case of a constant bifurcation parameter, and likewise triggers an early tipping when the drifting rate of the bifurcation parameter is slow enough. A brief comparison of the additive noise and the periodic forcing cases is also shown. In section 4, we show that the position of the tipping point is affected by the frequency, amplitude, and phase of the low frequency oscillation. For

the case where the frequency of the oscillatory forcing is the same order of magnitude as the drifting rate of the bifurcation parameter, we develop an analysis based on the local concavity of the trajectory to find the threshold of the amplitude at which there is an abrupt change of the position of the tipping point. Then we adapt this analysis to consider cases forced by a periodic oscillation with low frequency that is larger than the drifting rate of the bifurcation parameter. For consideration of the system with large amplitude, we study a rescaled model to which the analysis from the low or high frequency cases can be applied for certain parameter combinations. In sections 5 and 6 we consider two models with saddle node–type bifurcations, transformed to be similar to the canonical model. Then we can directly apply the approaches from the previous sections to determine the tipping points in these examples.

Throughout the paper we compare our analytical results to simulations of the model using a second order Runge–Kutta method, except for the Morris–Lecar model in section 5, where we use a fourth order Runge-Kutta method.

2. The canonical model.

We consider a canonical model with additive periodic forcing,

$$\begin{aligned} &\frac{\mathrm{d}x}{\mathrm{d}t} = a - x^2 + A\sin(\Omega t), \quad \frac{\mathrm{d}a}{\mathrm{d}t} = -\mu, \\ &\qquad x(0) = x_0,\ a(0) = a_0 > 0, \end{aligned} \tag{1}$$

where $a(t)$ denotes the slowly varying bifurcation parameter with the drifting rate $0 < \mu \ll 1$, A is the amplitude of the oscillation ($A > 0$), and Ω represents the frequency. We assume a_0, A are positive constants and $x_0 = \sqrt{a_0}$.

The system (1) is generalized from the canonical model for a saddle node bifurcation when $a(t)$ is a constant and $A = 0$ [25]. For any constant $a > 0$, there exist a stable equilibrium $x_e^+ = \sqrt{a}$ and an unstable equilibrium $x_e^- = -\sqrt{a}$. For $a < 0$, no equilibrium exists and the trajectory of (1) decreases exponentially for any initial condition x_0. The bifurcation diagram is shown in Figure 1.

For the system (1) without the periodic forcing term ($A = 0$), there is no equilibrium because $a(t)$ is slowly varying. With initial conditions x_0 and $a_0 > 0$, the trajectory of the system is exponentially attracted to one specific solution which we call the slowly varying equilibrium solution, analyzed in [9, 15] for $A = 0$, which we briefly summarize here. For $a(t) > 0$, the slowly varying equilibrium solution is close to $x = \sqrt{a}$ for a constant, which we call the stable branch throughout this paper. As $a(t)$ crosses zero, there is a transition from the slowly varying equilibrium solution to the rapidly decreasing behavior. This transition occurs for the value $a(t)$ below the static saddle node bifurcation point at $a = x = 0$, and thus is called a delayed bifurcation (see [9] and references therein). When such an abrupt qualitative change occurs, it is often referred to as a tipping point regardless of the value of $a(t)$. The method of matched asymptotic expansions is applied to find the approximation of the slowly varying equilibrium solution for $A = 0$ [9, 16], using a slow time scale μt and solving for $x(t)$ as a function of $a(\mu t)$,

$$x(a(\mu t)) = \sqrt{a} + \frac{\mu}{4a} - \frac{5}{32}\frac{\mu^2}{a^{5/2}} + O(\mu^3), \tag{2}$$

for $a(\mu t) \sim O(1)$. Notice that if $a(\mu t)$ is $O(\mu^{2/3})$, the terms shown in (2) are all $O(\mu^{1/3})$ and

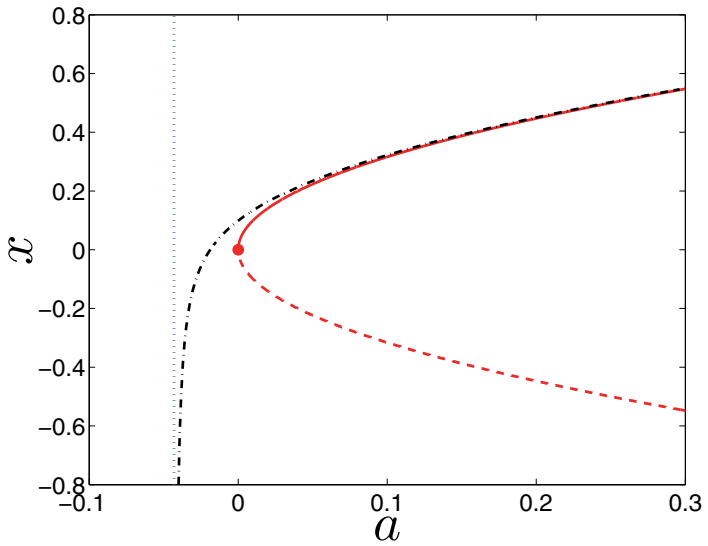

Figure 1. *The asymptotic approximation of the slowly varying equilibrium solution (2), (3) of the system (1) without periodic forcing ($A = 0$) (black dash-dotted line) is compared with the saddle node bifurcation diagram (red solid and dashed lines). The solid (dashed) line is the stable (unstable) steady state. The solid circle indicates the static bifurcation point. The vertical blue dotted line indicates the value of a_d (4), the singularity of (3). The drifting rate is $\mu = 0.0025$.*

the expansion is no longer valid. Then a local approximation is needed, which yields

$$x(a(\mu t)) \sim -\mu^{1/3}\frac{\mathrm{Ai}'(a/\mu^{2/3})}{\mathrm{Ai}(a/\mu^{2/3})}, \tag{3}$$

where Ai denotes the Airy function. The asymptotic approximation of the slowly varying equilibrium solution of (1) with $A = 0$ is shown in Figure 1, and compared with the static saddle node bifurcation diagram. The tipping happens near the singularity in the expression (3), which is the first zero of the Airy function,

$$a_d = \mu^{2/3} \cdot (-2.33810...)\,. \tag{4}$$

The smaller μ is, the slower $a(t)$ varies, and the closer the tipping point is to the static bifurcation value $a = 0$. The $\mu^{2/3}$ law characterizes the delay of the jump transition and has been verified experimentally in various physical systems [26, 27, 28]. This scaling law reappears throughout the results in this paper, due to the parabolic nature of the bifurcation structure near a saddle node bifurcation.

For $A > 0$ in (1), we explore the effect of the amplitude and frequency of the oscillation on the location of the tipping point, considering both high and low frequency in combination with the slow drift of the parameter $a(t)$.

3. High frequency oscillation $\Omega \gg 1$. In order to see how the tipping location is influenced by high frequency periodic forcing, we first consider (1) with constant a ($\mu = 0$) and determine the critical value of the bifurcation parameter where the bounded attracting

solution loses stability. We identify this bifurcation point denoted a_p, analogous to the saddle node bifurcation point in section 2, using the methods of multiple scales and matched asymptotic expansions. This result shows that the periodic forcing shifts the location of the bifurcation point to a value of $a > 0$. We compare this effect with the shift in the location of the tipping point for combined slowly varying $a(t)$ and high frequency forcing. We obtain an expression for this shift in terms of the drifting rate μ of $a(t)$, the frequency Ω, and the amplitude A. First we consider values of A smaller than Ω or of the same order of magnitude of Ω. For larger values of A, a different approach is needed, as shown in section 3.3.

3.1. Constant bifurcation parameter. For $\mu = 0$ ($a(t)$ a constant) and $A \neq 0$, the solution of (1) oscillates periodically around $\sqrt{a}$ for a an $O(1)$ constant, but it exponentially decreases for parameter values below the bifurcation value of $a = a_p$. We locate a_p, using the method of multiple scales [22], based on both a fast time scale $T = \Omega t$ and the original $O(1)$ time scale t, the slow time scale in this case. For $x = x(T, t)$, (1) becomes

$$x_T + \Omega^{-1} x_t = \Omega^{-1} a - \Omega^{-1} x^2 + \Omega^{-1} A \sin(T), \text{ where } x_T = \frac{\partial x}{\partial T}, \; x_t = \frac{\partial x}{\partial t}, \tag{5}$$

and the expansion

$$x \sim x_0(T, t) + \Omega^{-1} x_1(T, t) + \Omega^{-2} x_2(T, t) + \cdots \tag{6}$$

is substituted into (5), yielding

$$O(1) : x_{0T} = 0, \tag{7}$$

$$O(\Omega^{-j}) : x_{jT} = R_j(T, t), \;\; j = 1, 2, 3, \ldots. \tag{8}$$

The leading order equation (7) indicates that $x_0 = x_0(t)$, so that x_0 depends only on the slow time variable t.

To find x_j for $j = 0, 1, 2, \ldots$, we use a solvability condition to eliminate secular terms in the solution of (8) that monotonously increase in the fast time variable T. The solvability condition is that the right-hand side of (8) is orthogonal to the homogeneous solution of $x_{jT} = 0$ [22],

$$\lim_{T \to \infty} \frac{1}{T} \int_0^T R_j(u, t) du = 0, \;\; j = 1, 2, 3, \ldots. \tag{9}$$

Under the assumptions of the method of multiple scales, t and T are treated as independent variables. For $j = 1$,

$$R_1(T, t) = a - x_0^2 - x_{0t} + A \sin(T). \tag{10}$$

By applying the solvability condition (9) on (10), we have

$$\begin{aligned} x_{0t} &= a - x_0^2, \quad &\Rightarrow \quad x_0 &= \sqrt{a}, \\ x_{1T} &= A \sin(T), \quad &\Rightarrow \quad x_1 &= -A \cos(T) + v_1(t), \end{aligned} \tag{11}$$

where $v_1(t)$ is a function that needs to be determined in the higher order analysis.

The higher order corrections x_j, $j = 2, 3$, are obtained in Appendix A, yielding the asymptotic approximation for the attracting solution of (1) for $\mu = 0$, a a constant, as

$$x \sim \sqrt{a} + \Omega^{-1} \cdot [-A\cos(T)] + \Omega^{-2} \cdot \left[2\sqrt{a}A\sin(T) - \frac{A^2}{4\sqrt{a}}\right] + \cdots . \tag{12}$$

Similarly, one can find the approximation of the solution for the case when $x_0 = -\sqrt{a}$ and show it to be unstable.

For $A = 0$, (12) reduces to $x = \sqrt{a}$ with a saddle node bifurcation point at $a = 0$. For $A > 0$, (12) is valid when both A and a are $O(1)$. For $a = O(\Omega^{-2})$, we substitute $a = \Omega^{-2}b$ and introduce the expansion (6) into (5) to find a_p. In Appendix A, we find the leading order approximation of the attracting solution for $a = O(\Omega^{-2})$,

$$x \sim \sqrt{a - \frac{A^2}{2\Omega^2}} - \frac{A}{\Omega}\cos(T) + \cdots . \tag{13}$$

For a a constant, (13) shows that there are no attracting solutions if $a < a_p = A^2/(2\Omega^2)$.

3.2. High frequency oscillation in a slowly varying system. For $a(t)$ as in (1) with $\mu \ll 1$, we introduce a new parameter $\lambda > 0$ by writing $\Omega = \mu^{-\lambda}$ in (1). The parameter λ captures the relationship between frequency and drifting rate, which we relate to the tipping point below. Here we consider the case $A = o(\Omega)$ for $\Omega \gg 1$, and we consider larger values of A in section 3.3. To obtain an expression for the tipping location, we use a combination of the method of multiple scales together with outer and local expansions. The outer expansion does not provide the location of the tipping point, but it indicates a new scaling for a local analysis. In the local analysis we use a different combination of multiple scales and obtain an expression for the tipping point in terms of the key parameters.

For the outer approximation, we find it is sufficient to use two scales, the fast time scale $T = \mu^{-\lambda}t$ from the oscillatory forcing and the slow time scale $\tau = \mu t$ of the parameter $a(\tau)$. In terms of these time scales, (1) becomes

$$\begin{aligned} \mu^{\lambda+1}x_\tau + x_T &= \mu^\lambda \left[a - x^2 + A\sin(T)\right], \\ a_\tau &= -1. \end{aligned} \tag{14}$$

By substituting the general expansion

$$x \sim x_0(T, \tau) + \mu^\lambda x_1(T, \tau) + \mu^{2\lambda} x_2(T, \tau) + \cdots \tag{15}$$

into (14) and solving for each order by applying the solvability condition (9) (details shown in Appendix B), we get the asymptotic approximation of x for $a(\tau) = O(1)$,

$$x \sim \sqrt{a} + \frac{\mu}{4a} + \mu^\lambda \left[-A\cos(T)\right] + \cdots . \tag{16}$$

This result is similar to (2), with an oscillatory correction term $\mu^\lambda [-A\cos(T)]$ from the high frequency oscillatory term in (1). The asymptotic approximation (16) describes the attracting solution of (1) away from $a = 0$, but does not describe tipping. As $a(t)$ approaches zero,

specifically for $a(t) \sim O(\mu^{2/3})$, the first two terms are both $O(\mu^{1/3})$ so that the expansion (16) is not valid. In order to determine the influence of the oscillations on the location of the tipping point compared to (4), a local analysis for $a(t) \sim O(\mu^{2/3})$ is needed.

For the local analysis, we introduce $a(t) = \mu^{2/3}\alpha(s)$, the fast time variable $T = \mu^{-\lambda}t$ and a new slow time variable $s = \mu^{1/3}t$, and substitute into (1). The system (1) becomes

$$\begin{aligned} \mu^{1/3+\lambda}x_s + x_T &= \mu^{\lambda+2/3}\alpha - \mu^{\lambda}x^2 + \mu^{\lambda}A\sin(T), \\ \alpha_s &= -1, \end{aligned} \tag{17}$$

and we focus on the local equation (17) to determine the location of the tipping point. Separate analyses for different values of λ suggest that it is useful to substitute $x = -\mu^{\lambda}A\cos(T) + \mu^{1/3}y(T,s)$ in (17), yielding the asymptotic result for $\frac{1}{3} \le \lambda < 1$. Then we get

$$\mu^{\lambda+1/3}y_s + y_T = \mu^{\lambda}[\mu^{1/3}\alpha - \mu^{2\lambda-1/3}\frac{A^2}{2} - \mu^{2\lambda-1/3}\frac{A^2}{2}\cos(2T) + 2\mu^{\lambda}Ay\cos(T) - \mu^{1/3}y^2] \tag{18}$$

and substitute the expansion

$$y \sim y_0(T,s) + \mu^{\lambda+1/3}y_1(T,s) + \cdots \tag{19}$$

into (18), yielding $y_0 = y_0(s)$, and

$$O(\mu^{\lambda+1/3}) : y_{1T} = -y_{0s} + \alpha - \mu^{2\lambda-2/3}\cdot\frac{A^2}{2} - \mu^{2\lambda-2/3}\cdot\frac{A^2}{2}\cos(2T) + \mu^{\lambda-1/3}\cdot 2Ay\cos(T) - y_0^2. \tag{20}$$

We apply the solvability condition (9) to (20), yielding

$$y_{0s} = \alpha - y_0^2 - \mu^{2\lambda-2/3}\frac{A^2}{2}, \;\Rightarrow\; y_0 = -\frac{\mathrm{Ai}'(\alpha - \mu^{2\lambda-2/3}\cdot\frac{A^2}{2})}{\mathrm{Ai}(\alpha - \mu^{2\lambda-2/3}\cdot\frac{A^2}{2})}. \tag{21}$$

The local approximation of the attracting solution for $a = O(\mu^{2/3})$ is given by

$$x \sim \mu^{\lambda}\cdot[-A\cos(\Omega t)] + \mu^{1/3}\cdot\left[-\frac{\mathrm{Ai}'[(a-\mu^{2\lambda}\frac{A^2}{2})/\mu^{2/3}]}{\mathrm{Ai}[(a-\mu^{2\lambda}\frac{A^2}{2})/\mu^{2/3}]}\right] + \cdots. \tag{22}$$

For $\frac{1}{6} < \lambda < \frac{1}{3}$, we substitute the expansion (15) into (17) and get the same approximation as (22) in the end. For $\lambda \le \frac{1}{6}$, the frequency is treated as $O(1)$ and is not considered here.

Comparing (22) with (3), and recalling the relationship $\Omega = \mu^{-\lambda}$, we find that the position of the tipping point is determined by a that satisfies $\mathrm{Ai}[(a - \frac{A^2}{2\Omega^2})/\mu^{2/3}] = 0$. Then the tipping point with high frequency forcing and slowly drifting bifurcation parameter is given by

$$a_{\mathrm{hf}} \sim a_d + a_p = \mu^{2/3}K + \frac{A^2}{2\Omega^2} \tag{23}$$

for K given in (4) and a_p giving the same shift due to the periodic forcing as observed for the bifurcation point in (13) for $\mu = 0$. Recall that in this section we consider the case $A = o(\Omega)$, with larger values of A discussed below.

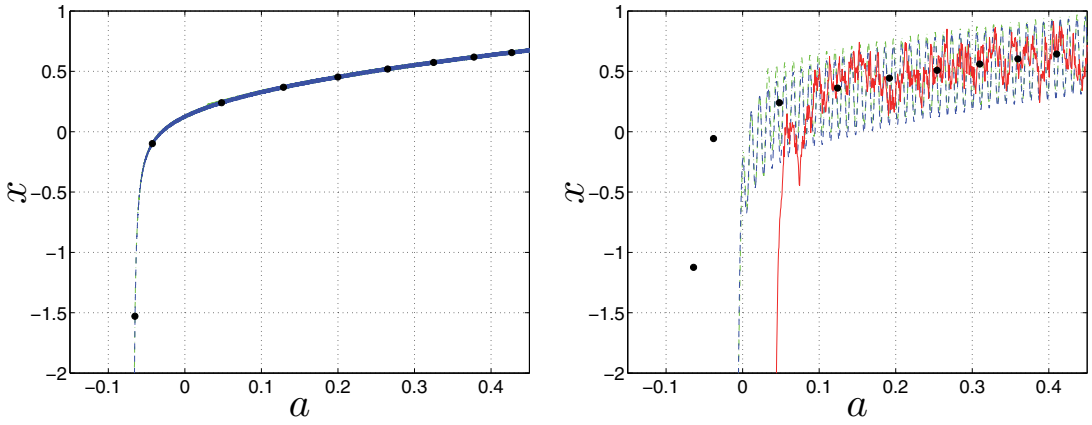

Figure 2. *Tipping is shown for $\mu = 0.005$. Left: The asymptotic approximations of the attracting solution for $A = 1$ and $\lambda = 0.8$; (16) (including higher order corrections up to $O(\mu^{3\lambda})$) and (22) (blue dashed line) are consistent with the trajectory generated numerically (green dash-dotted line). The position of the tipping point is compared with the case of $A = 0$ (black heavy dots). Right: Blue dashed and green dash-dotted lines as on the left with $A = 1$ and $\lambda = 0.2$, compared with the numerical simulation for the stochastic process obtained by replacing the periodic forcing by an additive white noise (red solid line). The noise coefficient is $\epsilon = 0.2$ for the realization shown.*

Figure 2 shows the effect of the high frequency oscillation in (1) on the location of the tipping point. For higher frequency the location is almost the same as the case with no oscillation, but for lower frequency (smaller values of λ) there is earlier tipping. We also see that a slower oscillatory forcing in (1) results in a larger amplitude oscillation around the slowly varying equilibrium solution found without oscillatory forcing (2), consistent with the expression for the outer approximation (16).

In [15, 16], it was shown that early tipping can be triggered also by white noise, in the system obtained by replacing the periodic forcing in (1) with an additive white noise, specifically, $dx = (a - x^2)\,dt + \epsilon dW(t)$ for $W(t)$ a standard Brownian motion. Early tipping is shown to occur with nonnegligible probability for noise amplitude $\epsilon = O(\mu^{1/2})$ or larger. For the shifted tipping points shown in Figure 2 (right) resulting from noisy and periodic forcings, the amplitude of the oscillatory forcing ($A = O(1)$) is an order of magnitude larger than the noise coefficient ($\epsilon = o(1)$) that generates a comparable advance of tipping. The probability of early escape, corresponding to x crossing the unstable branch, is in the range $0.25 < P(x < -\sqrt{a}) < 0.43$ for a varying between $a = 0.05$ and $a = 0.025$ for the parameters shown here. An asymptotic approach for the corresponding time-dependent probability density function is given in [17].

In contrast, for high frequency periodic forcing, it is the ratio of amplitude to frequency that plays a significant role in shifting the tipping point location, rather than the magnitude of the amplitude alone. The asymptotic approximation for the tipping point location $a_{\rm hf}$ given in (23) is compared with numerical simulations in Figure 3 for different drifting rates μ and varying exponent λ for $\Omega = \mu^{-\lambda}$. There we see the competition between the two components in $a_{\rm hf}$. For $A = 1$ and smaller values of μ, that is, slower drifting rates, the location of the tipping point is dominated by a_d corresponding to $A = 0$ (4). In those cases only for smaller

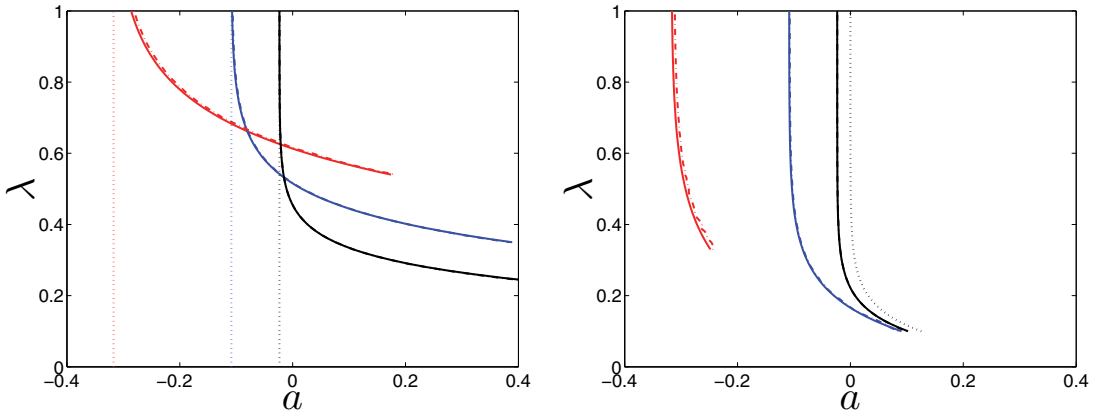

Figure 3. *The position of the tipping point for different frequencies $\Omega = \mu^{-\lambda}$, shown for three drifting rates μ. At $\lambda = 1$ the values of μ shown decrease from left to right in both panels: $\mu = 0.05$ in red; $\mu = 0.01$ in blue; $\mu = 0.001$ in black. The asymptotic approximation (23) is shown by the solid line. The dash-dotted line shows the location of the tipping point obtained from numerical simulations, defined as the value of a for $x = -10$. Left: $A = 5$; the dotted vertical lines show the position of the tipping point a_d for $A = 0$. Right: $A = 1$; the black dotted line shows the approximation of the bifurcation point $a_p = A^2/(2\Omega^2)$ for $\mu = 0$.*

values of λ, that is, lower frequencies, is there a noticeable influence of the periodic term, as seen in Figure 3 (right). The advance of $a_{\rm hf}$ due to the periodic forcing as captured by a_p clearly increases with A. For example, the case $A = 5$ is shown in Figure 3 (left), where there are larger advances associated with a_p for decreasing λ, as compared with negligible advances for $A = 1$ and smaller λ. As noted above, for smaller values of λ (near $\lambda \approx 1/3$ or below), the frequency Ω of the oscillatory forcing is not necessarily large, depending on the value of μ. Then the expansion (15) is no longer a reasonable asymptotic approximation, and instead the behavior has some of the features discussed in section 4 for low frequency forcing. As seen in Figure 3, the asymptotic approximation is valid for a larger range of λ for smaller values of μ. The approximation $a_{\rm hf}$ and (22) break down for $A \sim O(\Omega)$, since the coefficient $\mu^{2\lambda}A^2 = A^2/\Omega^2$ that appears in (20)–(22) and in the argument of Ai is treated as $o(1)$ to obtain $a_{\rm hf}$. We consider results for larger values of A separately in the next section.

3.3. High frequency oscillation with large amplitude ($A \gg 1$). In sections 3.1 and 3.2, the asymptotic approximations (16) and (22) are not valid if $A = O(\Omega)$ or larger. However, for some larger values A and frequency Ω, we can rescale (1) to obtain a similar system forced by an oscillation with amplitude of unity. In certain cases we can apply the approximations from either section 3.2 or section 4.1 to the rescaled system.

Substituting $x = \sqrt{A}z$ and $t = S/\sqrt{A}$ into (1), we get

$$\begin{aligned} \frac{\mathrm{d}z}{\mathrm{d}S} &= h - z^2 + \sin(\omega S), \\ \frac{\mathrm{d}h}{\mathrm{d}S} &= -M, \\ v(0) = v_0 = \frac{x_0}{\sqrt{A}}, &\qquad h(0) = h_0 = \frac{a_0}{A}, \end{aligned} \tag{24}$$

where $\omega = \Omega/\sqrt{A}$, $h = \frac{a}{A}$, and $M = A^{-3/2}\mu$ are the scaled frequency, bifurcation parameter, and drifting rate, respectively. In order to consider the case $A \gg 1$, we assume $A = \Omega^P$ with $P \geq 1$. Then the relationship between ω and M is given by $\omega = M^\zeta$, with ζ a function of λ and P:

$$\zeta = \frac{P-2}{3P + 2/\lambda}. \tag{25}$$

For $1 \leq P < \frac{4}{3}$, the high frequency approximation (22) can be applied to (24) if $\zeta < -\frac{1}{6}$, which indicates that λ in $\Omega = \mu^{-\lambda}$ satisfies $\lambda > \frac{2}{12-9P} \geq \frac{2}{3}$. For larger values of A ($P \geq \frac{4}{3}$), the oscillatory forcing and the drifting bifurcation parameter both dominate the dynamics to leading order, so that the asymptotic approximation (16) dominated by the slowly drifting parameter $a(t)$ is no longer valid.

For $P > 2$ and $\lambda > 0$, ζ is positive, which indicates that even though (1) has a high frequency oscillatory forcing, in the normalized system (24) the relationship between ω and M corresponds to a low frequency case, discussed in the next section. We note that ζ is a monotone increasing function with respect to P with a horizontal asymptote at $\zeta = \frac{1}{3}$.

4. Low frequency oscillation $\Omega \ll 1$. For the case of a low frequency oscillation ($\Omega \ll 1$), we introduce a new parameter $\nu > 0$ by writing $\Omega = \mu^\nu$, capturing the relationship between the frequency and the drifting rate. In the following we consider two different cases: $\nu \geq 1$ so that $\Omega = O(\mu)$ or smaller, or $\Omega = \mu^\nu$ with $0 < \nu < 1$. Unlike the high frequency case, for low frequency oscillations we cannot use the method of multiple scales, since the key time scales of drifting and the frequency are both slow. Then the asymptotic approach relies on understanding the local behavior of the trajectory that is driven by the slow oscillations.

4.1. $\Omega = O(\mu)$ or smaller. Here it is convenient to write $\Omega = c\cdot\mu$ for c a positive constant and to write the system in terms of $\tau = \mu t$, expressing x as a function of $a(\tau) = a_0 - \tau$ in (1), to get

$$-\mu\frac{dx}{da} = f(a) - x^2 = a - x^2 + A\sin(c\cdot(a_0 - a)). \tag{26}$$

Substituting $x \sim x_0 + \mu x_1 + \mu^2 x_2 + \cdots$ into (26), we find the first two terms of the approximate solution as a function of $a(\tau)$:

$$\begin{aligned} x &\sim \pm\sqrt{f(a)} + \mu\cdot\frac{f'(a)}{4f(a)} + \cdots \\ &\sim \pm\sqrt{a + A\sin(c\cdot(a_0 - a))} + \mu\cdot\frac{1 - c\cdot A\cos(c\cdot(a_0 - a))}{4(a + A\sin(c\cdot(a_0 - a)))} + \cdots, \end{aligned} \tag{27}$$

where the positive sign corresponds to the solution that is attracting. Note that the oscillatory term appears in the leading order contribution in (27), in contrast to the leading order approximation in the case of the high frequency oscillations (16), where there is no oscillatory term. Similar to (2), the terms shown in (27) are both $O(\mu^{1/3})$ for $f(a) \sim O(\mu^{2/3})$ and the expansion is no longer valid. Then we expect a tipping point near $a = a_r$, where $f(a) > 0$ for $a > a_r$ and $f(a_r) = 0$. A local analysis near $a = a_r$ is used to determine the location

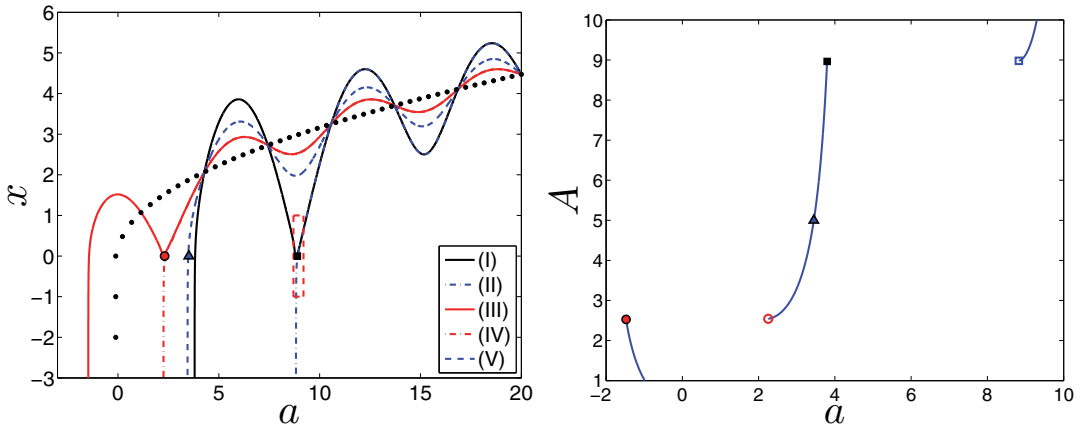

Figure 4. *Parameter values are* $\mu = \Omega = 0.01$ *(*$c = 1$*),* $a_0 = 20$ *for all graphs. Left: Numerical simulation of* (1)*. The Roman numerals correspond to cases with different values of A: Case* (I)*,* $A = 8.9647$*; Case* (II)*,* $A = 8.9797$*; Case* (III)*,* $A = 2.5268$*; Case* (IV)*,* $A = 2.5418$*; Case* (V)*,* $A = 5$*. With the exception of Case* (V)*, A is near the critical value* A_c *at which there is an abrupt change of the tipping position. Heavy black dots:* $A = 0$*. The solid black square (red circle) corresponds to parameter values* $(a, A) = (a_m, A_m)$*, in Cases* (I) *and* (II) *(Cases* (III) *and* (IV)*), with* A_m *taking values slightly less than the value of A for Cases* (I)–(IV)*. The dashed rectangle indicates the region shown on a larger scale in Figure* 5 *(left). The blue triangle marks the value of* a_r *where* $f(a_r) = 0$ *for* $A = 5$*. Right: The location of the tipping point as a function of A in* (1) *obtained by numerical simulations, with tipping defined as the value of a where* $x = -10$ *as in the previous cases. Different markers indicate the value of A and corresponding tipping point value, for the trajectories shown in the left panel. Solid (black) square:* (I)*; open (blue) square:* (II)*; solid (red) circle:* (III)*; open (red) circle:* (IV)*; solid (blue) triangle:* (V)*.*

of the tipping point. In our analysis and simulations we take $a_0 > a_r$ for $f(a_r) = 0$ with $|a_0 - a_r| = O(1)$, ensuring that the system (1) attracts to the outer solution (27) prior to any tipping.

Figure 4 shows numerical simulations of (1) for different values of A and fixed a_0, illustrating important characteristics of tipping that are the basis for our analysis. The heavy black dots correspond to $A = 0$ (no modulations). For larger values of A, the trajectory $x = x(a)$ exhibits larger oscillations and exhibits tipping before a reaches or crosses the static bifurcation value at $a = 0$. As could be expected, the value of a where the tipping occurs increases with A for $a > 0$. For amplitudes A where the trajectory crosses $x = 0$ for $a(t) > 0$, tipping can occur well before the static bifurcation point is reached. Abrupt shifts in tipping point location are observed for critical amplitudes denoted A_c that are slightly greater than A_m, where the pair $(a, A) = (a_m, A_m)$ satisfies $f(a_m) = f'(a_m) = 0$ as discussed below (31). For example, the Cases (I) and (II) shown in Figure 4 (left) have the values of $A = 8.9647$ and $A = 8.9797$, respectively, with both values slightly greater than $A_m \approx 8.9485$ for $a_0 = 20$. However, the tipping for Case (I) occurs at $a \approx 3.80$ (solid black square in Figure 4 (right)), while the tipping for Case (II) occurs at $a \approx 8.82$ (open blue square in Figure 4 (right)). Here the value of a_m is indicated by the solid black square in Figure 4 (left), which is near the tipping point for Case (II) but not for Case (I). This figure illustrates how amplitudes $A > A_c$ cause an early tipping near a value of a where $x < 0$, while for the same initial condition and $A < A_c$, the periodic forcing is not sufficient to drive tipping at the same value of a as for

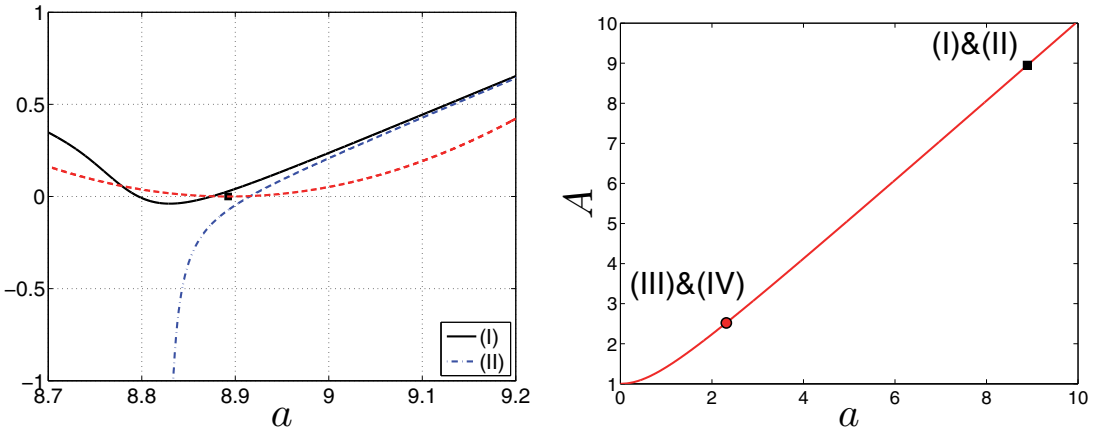

Figure 5. *For all graphs,* $\mu = \Omega = 0.01$ *(*$c = 1$*). Left: Figure 4 (left) zoomed in near* a_m *for* $f'(a_m) = 0$ *(black square), with* $f(a)$ *for* $a_0 = 20$ *and* $A = A_m = 8.9485$ *given by the red dashed curve. Numerical simulations of Case* (I) *(solid black line,* $A = 8.9647$*) and Case* (II) *(dash-dotted blue line,* $A = 8.9797$*) are also shown. Right:* A_m *as a function of* a_m *(solid red line), with* a_0 *varying along this line as in* (31) *and* (32)*. The black square (red circle) marks the value of* a_m *and* A_m *for Cases* (I) *and* (II) *(Cases* (III) *and* (IV)*), with* $a_0 = 20$ *as in Figure 4.*

$A > A_c$. Rather, the oscillations continue for another period, with tipping likely to take place near the next crossing of $x = 0$. Figure 4 (right) shows the location of the tipping points for all trajectories represented in Figure 4 (left) and indicates the critical values A_c where there are abrupt changes in the tipping point as a function of A. Note that the tipping points for $A < A_c$ and $A > A_c$ may both correspond to early tipping relative to the static bifurcation $a = 0$ and to the unforced delayed bifurcation $a = a_d$ in (4), as is true for Cases (I) and (II). For smaller values of A_c, such as the value near Cases (III) and (IV), amplitudes $A > A_c$ drive early tipping at $a > 0$ (Case (IV)), while $A < A_c$ drives tipping at $a < 0$, delayed relative to $a = 0$ and $a = a_d$ (Case (III)). As we study separately below, the values A_c are near A_m, and are related to the local behavior of the trajectory near a_m. Figure 5 (left) zooms in on the trajectories (I) and (II) near $a = 8.9$ and illustrates the obvious change of concavity near a_m, which proves to be an essential part in estimating A_c.

Before we investigate the solution near (a_m, A_m) where $f(a_m) = f'(a_m) = 0$ (and near A_c), we first consider the case where tipping occurs close to $a = a_r$, where $f(a_r) = 0$ and $f'(a_r) = O(1)$, as in case (V) in Figure 4 (left). Near $a = a_r$, specifically $f(a) = O(\mu^{2/3})$, we substitute $a - a_r = \mu^{2/3}B$ and $x = \mu^{1/3}X$ into (26), yielding

$$O(\mu^{2/3}) : -X_B = f'(a_r)B - X^2 = [1 - cA\cos(c \cdot (a_0 - a_r))]B - X^2, \tag{28}$$

which has the solution for $f'(a_r) \neq 0$,

$$X = -C^{1/3}\frac{\mathrm{Ai}'(C^{1/3}B)}{\mathrm{Ai}(C^{1/3}B)}, \;\Rightarrow\; x = -(\mu C)^{1/3}\frac{\mathrm{Ai}'((C/\mu^2)^{1/3}(a - a_r))}{\mathrm{Ai}((C/\mu^2)^{1/3}(a - a_r))}, \qquad C = f'(a_r). \tag{29}$$

Similar to the analysis for (3) and (22), the location of the tipping point is determined by the singularity of (29) where $\mathrm{Ai}((C/\mu^2)^{1/3}(a - a_r)) = 0$, which is

$$a_{lf} = a_r + a_d/(f'(a_r))^{1/3} \text{ for } f(a_r) = 0 \text{ and } f(a) > 0 \text{ for } a > a_r, \tag{30}$$

where a_d is given in (4). We differentiate $f(a_r) = 0$ with respect to A to obtain $da_r/dA = (CA)^{-1}a_r$, which indicates that the location of the tipping point increases (decreases) with increasing A for a_r negative (positive), as shown in Figures 4 (right) and 7 (right).

Noting that (29) is obtained from (28) for $f'(a_r) \neq 0$, we propose a separate analysis for (a, A) close to (a_m, A_m), which satisfy the conditions

$$f(a_m) = a_m + A_m \sin(c \cdot (a_0 - a_m)) = 0, \tag{31}$$

$$f'(a_m) = 1 - cA_m \cos(c \cdot (a_0 - a_m)) = 0 \;\Rightarrow\; c^2 a_m^2 + 1 = c^2 A_m^2. \tag{32}$$

The behavior of $f(a)$ near a_m for $A = A_m$ is shown in Figure 5 (left). Figure 5 (right) shows A_m as a function of a_m for different values of a_0 as in (31) and (32). From these conditions, we see that for each a_0 there is a family of initial values $a_0 + \frac{2k\pi}{c}$ for k an integer that corresponds to the same pair (a_m, A_m). Equations (31) and (32) indicate that $A_m > 1/c$ and $0 < a_m < A_m$. We take $A > 0$ in (1), noting that similar results can be found for $A < 0$.

A comparison of Cases (I) and (II) in Figure 4 (left) with Figure 5 (left) suggests that the critical amplitude A_c, for which there is a jump in the location of the tipping point, is near A_m, with $A_c > A_m$. Furthermore, the trajectories shown in Figure 5 (left) have different concavities near $a = a_m$ for A above and below A_c. Specifically, for amplitudes $A > A_c$ for which an early tipping occurs, the trajectory is concave down near its crossing of $x = 0$. In contrast, if $A < A_c$, the trajectory is concave up near its crossing of $x = 0$ and no tipping occurs there, yielding oscillations for another period with tipping likely to take place near the next crossing of $x = 0$. Therefore, to find A_c and the corresponding tipping point, we consider the concavity of x in (26) with respect to a near a_m. Using (26), we write $x''(a)$ in terms of the local variables

$$a - a_m = \mu\eta, \qquad x = \mu\xi, \qquad \text{and } A = A_m + \mu A_1\,, \tag{33}$$

to focus on the neighborhood of $a = a_m$ and on amplitude values near A_m. Substituting the local variables (33) in (31) and (32), and expanding $\sin(c\mu\eta)$ and $1 - \cos(c\mu\eta)$ for $\mu \ll 1$, we obtain the leading order expression for the local concavity of $\xi(\eta)$:

$$\frac{d^2\xi}{d\eta^2} = \mu\left(\frac{A_1}{A_m} - c^2 a_m \eta + \frac{2A_1 a_m}{A_m}\xi\right) + O(\mu^2). \tag{34}$$

From (34) we find that the leading order expression of $\xi = x/\mu$ that separates trajectories of different concavities is given by

$$\xi_c = \frac{c^2 A_m}{2A_1}\eta - \frac{1}{2a_m}\,. \tag{35}$$

Then for $\xi > \xi_c$ ($\xi < \xi_c$), near $a = a_m$ the trajectory is concave up (down). To determine the critical value A_1 (and thus A_c) for which the trajectories change concavity, we compare (35) to the trajectory itself in terms of the local variables η, ξ, and A_1. The local expression for the trajectory ξ is found by substituting (33) into (26), and using the expansion $\xi \sim \xi_0 + \mu\xi_1 + \mu^2\xi_2 + \cdots$,

$$\xi \sim \frac{A_1 a_m}{A_m}\eta + c_0 + \mu\left[-\left(\frac{1}{2}c^2 a_m - \frac{A_1^2 a_m^2}{A_m^2}\right)\frac{\eta^3}{3} + \frac{A_1}{A_m}(1 + 2c_0 a_m)\frac{\eta^2}{2} + c_0^2\eta + c_1\right] + \cdots\,, \tag{36}$$

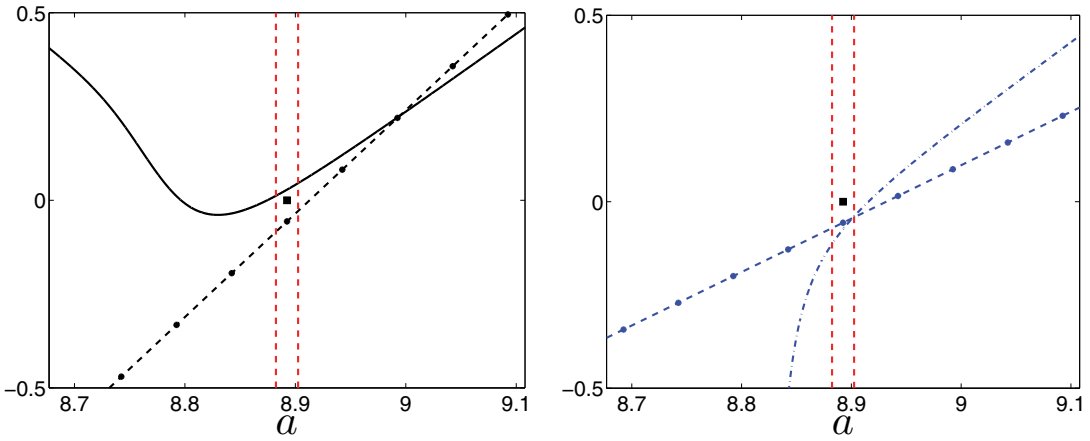

Figure 6. *View of Cases* (I) *and* (II) *as in Figure 4 (left), zoomed in on the scale* $|a - a_m| = \mu^{1/3}$, *with* $|a - a_m| = \mu$ *indicated by red dashed lines. The black square is the value of* a_m *where* $f(a_m) = f'(a_m) = 0$. *Left: The trajectory of Case* (I) *(solid black line) is compared with the concavity threshold* (35) *(black dashed line with markers). Right: The trajectory of Case* (II) *(blue dash-dotted line) is compared with the concavity threshold* (35) *(blue dashed line with markers).*

where c_0 and c_1 are undetermined constants. It is the comparison of the slope of the concavity threshold (35), $c^2 A_m/(2A_1)$, to that of the trajectory (36), $A_1 a_m/A_m$, that yields the result for A_1. If $A_1 a_m/A_m < c^2 A_m/(2A_1)$ for $a - a_m = O(\mu)$ and $x = O(\mu)$, then trajectories that enter the concave-up region stay there, as shown in Figure 6 (left), and tipping does not occur near $\eta = 0$ ($a = a_m$). Alternatively, if $A_1 a_m/A_m > c^2 A_m/(2A_1)$, then locally the trajectory has a slope greater than that of the concavity threshold, and trajectories that are near or below (35) for a near a_m cross into or continue in the concave-down region, resulting in tipping as shown in Figure 6 (right). Then the critical value of A_1 for the change in concavity satisfies

$$A_1^2 = \frac{\Omega c^2 A_m^2}{2\mu\sqrt{c^2 A_m^2 - 1}}, \quad c = \frac{\Omega}{\mu} \qquad \Rightarrow \qquad A_c \sim A_m + \mu A_1, \tag{37}$$

where we have used (32) to eliminate a_m and (33) to get A_c.

To arrive at (37), we assumed that for $A < A_c$, the trajectory (36) is above the concavity threshold (35) in the local region (33). To verify this assumption, we compare the ξ-intercept of the concavity threshold (35), $-\frac{1}{2a_m}$, to that of the trajectory, which to leading order is c_0. Then c_0 is determined by matching the local expansion (36) with the outer expansion (27), as shown in Appendix C,

$$c_0 = -\frac{1}{2a_m} + C_1 + C_2.$$

The ξ-intercept of the trajectory, relative to $-1/(2a_m)$, is obtained from the sign of $C_1 + C_2$. As discussed in Appendix C, for $\frac{A_1 a_m}{A_m} < \frac{c^2 A_m}{2A_1}$ ($\frac{A_1 a_m}{A_m} > \frac{c^2 A_m}{2A_1}$) we find that $C_1 + C_2 > 0$ ($C_1 + C_2 < 0$), which is consistent with our assumptions in the derivation of (37). Figure 6 illustrates the local behavior by comparing the trajectory and the concavity threshold near $a = a_m$.

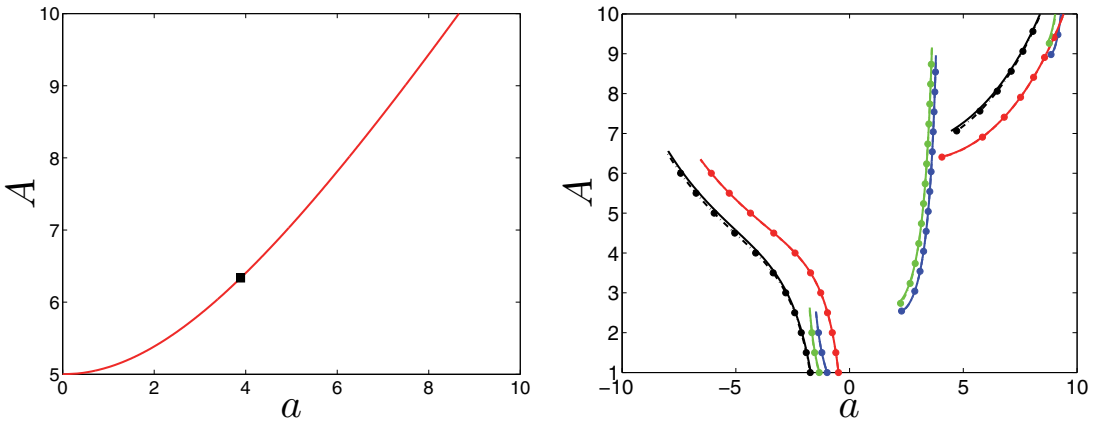

Figure 7. *Left: Values of A_m (red solid line) from (31) and (32) as a function of a_m for $c = 0.2$. The black square marks the value of a_m and A_m near parameter values where there is an abrupt change in the tipping point location, shown for the cases with $c = 0.2$ in the right panel. Right: The position of the tipping point as a function of amplitude A, comparing the asymptotic approximation (30) with jumps at values (37) (solid lines) with numerical simulation, defining the tipping point as the value of a when $x = -10$ (dash-dotted lines with markers). Different colors indicate different combinations of frequency Ω and drifting rate μ. Blue: $\Omega = 0.01$, $\mu = 0.01$, and $a_0 = 20$. Red: $\Omega = 0.01$, $\mu = 0.05$, and $a_0 = 32$. Green: $\Omega = 0.1$, $\mu = 0.1$, and $a_0 = 20$. Black: $\Omega = 0.1$, $\mu = 0.5$, and $a_0 = 32$.*

The panels in Figure 7 illustrate the dependence of these results on the ratio $c = \Omega/\mu$ and compare the tipping point locations obtained by asymptotic approximations (30) and (37) and by numerical simulations. The variation of A_m and A_c with the parameter c is observed by comparing the values of A_m shown in Figures 7 (left) and 5 (right), and noting the values of A_c where there is a jump in the location of the tipping point in Figure 7 (right). There we see that these jumps occur near $A = 9$ and near $A = 2$ for the cases with $c = 1$ (blue and green lines), in contrast to the cases with $c = .2$, where $6 < A_c < 7$ (red and black lines). Figure 7 also shows good agreement between results for the location of the tipping point as a function of A obtained from simulations and from the asymptotic approximation for $\Omega \ll 1$.

4.2. $\Omega = \mu^\nu$ $(0 < \nu < 1)$. For $c \gg 1$, so that the low frequency is large compared with the drifting rate, $\mu \ll \Omega \ll 1$, the approximation (37) is not valid since it is based on the assumption that $c = O(1)$. Nevertheless, simulation results shown in Figure 8 (left) for Ω relatively small illustrate phenomena similar to that shown in Figure 7 (right). As in the previous case of $\Omega = O(\mu)$, for a given a_0 there are values A_c at which there are abrupt shifts in the location of the tipping point as a function of the amplitude. These shifts are related to changes of concavity in the trajectory near a local minimum of $f(a)$ at $a = a_{\min}$, so that we can again use the concavity to identify A_c. As above, an early tipping occurs near a value of a where $x < 0$ for $A > A_c$, while for the same initial condition and $A < A_c$, oscillations continue for another period with tipping taking place on a future crossing of $x = 0$. There are also noticeable differences for $\Omega = \mu^\nu$, since the frequency is larger than in the previous section. For example, the consecutive crossings of $x < 0$ are closer together for larger frequencies, so that the shifts between tipping point location at $A = A_c$ decrease with ν and the values of A_c are closer together. Furthermore, $f(a_{\min}) < 0$ may be $O(1)$ for $a_{\min}$ near the tipping point,

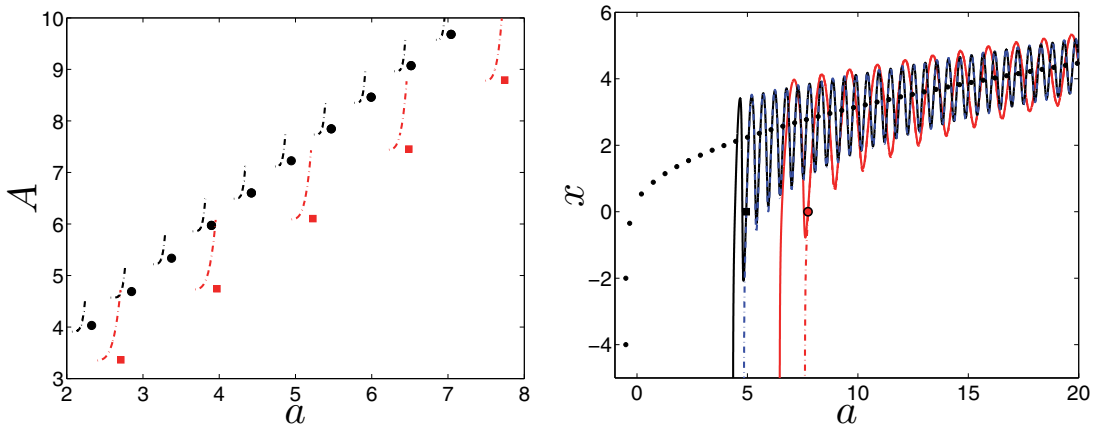

Figure 8. *The drifting parameter is $\mu = 0.1$ for all graphs. Left: Numerical simulations of the position of the tipping point (dash-dotted lines), defined as the value of a when $x = -10$, compared with markers indicating $(a_{\min}, A_c)$ from (44) and (45), the critical values of the amplitude at which there is an abrupt change in the location of the tipping point. Red dash-dotted line and solid squares are for the case $\Omega = 0.5$ and $a_0 = 20$. Black dash-dotted lines and solid circles are for the case $\Omega = 1.2$ and $a_0 = 20$. Right: Numerical simulation of (1) with A near A_c in the location of the tipping points in the left panel: $A = 8.7$ (red solid) and $A = 8.9$ (red dash-dotted), both with $\Omega = 0.5$; $A = 7.1$ (black solid line) and $A = 7.3$ (blue dash-dotted line), both with $\Omega = 1.2$. The black square and red circle mark the related $a_{\min}$ for $\Omega = 0.5, 1.2$, respectively, satisfying (44) and (45).*

in contrast to $f(a_m) = 0$ in section 4.1, as shown in Figure 5. As a result, we modify our approach for calculating A_c.

To approximate A_c for $\Omega = \mu^\nu$, we first consider the outer approximation to (26) given by (27) with $c = \mu^{\nu-1}$. As in section 4.1 this approximation is valid only for $f(a) > 0$, since as $f(a)$ approaches 0, the terms shown in (27) are both of the same order for $\mu \ll 1$. To estimate A_c in this case, we must consider multiple local minima $a_{\min}$ of $f(a)$ for a given a_0, satisfying

$$f(a_{\min}) = a_{\min} + A\sin(\mu^{\nu-1}(a_0 - a_{\min})) < 0, \tag{38}$$

$$f'(a_{\min}) = 1 - \mu^{\nu-1}A\cos(\mu^{\nu-1}(a_0 - a_{\min})) = 0, \;\Rightarrow\; \cos(\mu^{\nu-1}(a_0 - a_{\min})) = \mu^{1-\nu}\frac{1}{A}. \tag{39}$$

Since we are considering larger values of the frequency Ω, the values of $a_{\min}$ are relatively close together and close to values where $f(a) = 0$. Then we cannot use a local analysis near values of a where $f(a) = 0$, as was done near a_r in (28), but instead restrict our analysis near $a_{\min}$ for $f'(a_{\min}) = 0$.

Substituting $a = a_{\min} + \mu\eta$ and $x = \mu\xi$ into $x''(a)$ using (26), (38), and (39), we get the local expressions for the trajectory and its concavity. Keeping the terms that dominate these expressions for $\mu \ll 1$ yields

$$\mu\frac{d\xi}{d\eta} = -f(a_{\min}), \tag{40}$$

$$\mu\frac{d^2\xi}{d\eta^2} = \mu^{2\nu}(f(a_{\min}) - a_{\min})\eta - 2\mu f(a_{\min})\xi. \tag{41}$$

As in section 4.1, we look for the critical value of $A = A_c$ that corresponds to the value where the local slope of the trajectory is equal to that of the concavity threshold. The latter is obtained from setting $\xi''(\eta) = 0$ in (41), yielding

$$\xi_c = \frac{\mu^{2\nu}(f(a_{\min}) - a_{\min})\eta}{2\mu f(a_{\min})}. \tag{42}$$

Equating the coefficient of η from the right-hand side of (42) with $\xi'(\eta)$ in (40) gives the relation

$$-2f^2(a_{\min}) = \mu^{2\nu}(f(a_{\min}) - a_{\min}). \tag{43}$$

Then, using (38)–(39) and (43), we can eliminate $f(a_{\min})$ and obtain a system of equations for the pair $(a_{\min}, A_c)$,

$$a_{\min} = \sqrt{A_c^2 - \frac{\mu^2}{\Omega^2}} - \frac{\Omega}{\sqrt{2}}\left[A_c^2 - \frac{\mu^2}{\Omega^2}\right]^{1/4}, \tag{44}$$

$$a_{\min} = a_0 + \frac{\mu}{\Omega}\left[\cos^{-1}\left(\frac{\mu}{A_c\Omega}\right) - 2k\pi\right], \tag{45}$$

where k is a positive integer. Note that for fixed a_0 the system of equations (44)–(45) is valid for $\mu = o(\Omega)$. It has more than one solution, that is, more than one pair $(a_{\min}, A_c)$ at which there is a change in concavity and thus a jump in the location of the tipping point as a function of A. Then for small μ or sufficiently large A_c, $\cos^{-1}(\mu/(A_c\Omega)) \sim \pi/2$ in (45), so that the jumps in the value of $a_{\min}$ are dominated by $2k\pi\mu/\Omega$ for integers k, related to the multivalued function $\cos^{-1}(\cdot)$.

Figure 8 (left) compares the position of the tipping points obtained from numerical simulation with the asymptotic approximation for the critical values $a_{\min}$ and A_c given by (44)–(45). Figure 8 illustrates this approximation for $\mu = 0.1$, both for $\Omega = \mu^\nu$ for $\nu \approx 0.3$, and for $\Omega = O(1)$. While the latter case does not appear to be covered by the asymptotic analysis, we recall that in section 3.3 we showed that the case $A > \Omega^2$ with $\Omega = \mu^{-\lambda}$ for $\lambda > 0$ can be studied as a low frequency case by rescaling (1) into the normalized system (24). This rescaled system, with frequency $\omega < 1$ and slow drift parameter $M \ll 1$, can be analyzed using expressions analogous to (44)–(45). For $\frac{\mu}{\Omega} \ll 1$, we see that (44)–(45) provide a good approximation for the location of the tipping point and the values of A for which there is a jump in location, even though we do not have an analytical approximation for the solution x for $\Omega = O(1)$ and $\mu \ll 1$. For larger values of Ω with μ fixed, there are more values of A_c where this jump occurs, and the corresponding values of $a = a_{\min}$ are closer together. The increasing number and reduced distance between these jumps indicates that as Ω increases further, the relationship between the amplitude A and the location of the tipping point is a continuous function, as shown in section 3.2 for large frequency.

The analysis of large amplitude oscillatory forcing in section 3.3 suggests a rescaling of the system, which allows the asymptotic approximations to be extended to some cases where the frequency is not particularly large or small relative to the drifting rate of the bifurcation parameter. In Figure 9 we compare results for low, high, and O(1) frequencies Ω, illustrating how the location of the tipping point varies with the amplitude and frequency of the periodic forcing.

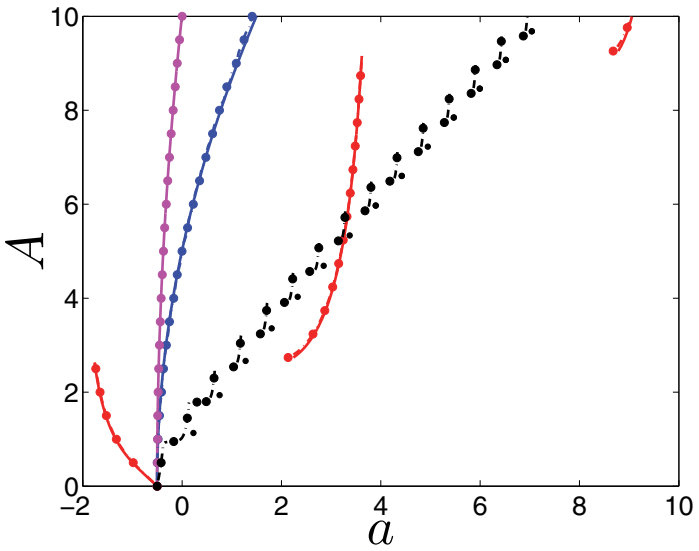

Figure 9. *Position of the tipping point as a function of A in (1) obtained by numerical simulation, defined as the value of a where $x = -10$ (dash-dotted line with solid circles) compared with the asymptotic approximation (solid line) for $\Omega = 0.1$ (red); $\Omega = 5$ (blue); and $\Omega = 10$ (magenta) with $\mu = 0.1$ and $a_0 = 20$. The black dash-dotted lines give the location of the tipping point determined numerically for $\Omega = 1.2$, which are compared with the black circles indicating the value of A where there is jump in the location of the tipping point based on the asymptotic approximation (44) and (45).*

5. Example 1: Morris–Lecar model. We consider the Morris–Lecar (ML) model [32, 34] with a slowly increasing input current and an additive periodic external input. The ML model has been used widely as a two-dimensional model, relatively straightforward to analyze, that captures certain dynamical behavior observed for different types of neurons with a variety of states. It has the general form

$$
\begin{aligned}
\gamma\frac{dv}{d\hat{t}} &= -g_{Ca}\hat{m}_\infty(v)(v-v_{Ca}) - g_K(v-v_K)w - g_L(v-v_L) + I_{\text{bias}} + I_{\text{ext}},\\
\frac{dw}{d\hat{t}} &= \hat{\kappa}(v)(\hat{w}_\infty(v) - w),\\
\frac{dI_{\text{bias}}}{d\hat{t}} &= \hat{\mu},\\
\hat{m}_\infty(v) &= \frac{1}{2}\left(1+\tanh\left(\frac{v-v_1}{v_2}\right)\right), \quad \hat{w}_\infty(v) = \frac{1}{2}\left(1+\tanh\left(\frac{v-v_3}{v_4}\right)\right),\\
\hat{\kappa}(v) &= \phi\cosh\left(\frac{v-v_3}{2v_4}\right),
\end{aligned}
\tag{46}
$$

where v represents the membrane voltage potential and w is the probability of opening of K^+ channels ($0 \le w \le 1$). This simplified model of excitability depends on three ionic currents for calcium, potassium, and leakage, described by the terms with the relevant conductances, g_{Ca}, g_K, and g_L. The periodic external input is I_{ext}, I_{bias} represents the bias or base current in the neuron, and we refer the reader to [33] for additional details. Here we take the commonly used

fixed constants as given in [34]: $v_K = -84\text{mV}$, $v_L = -60\text{mV}$, $v_{Ca} = 120\text{mV}$, $c = 20\mu\text{F/cm}^2$, $v_1 = -1.2\text{mV}$ and $v_2 = 18\text{mV}$, $g_K = 8\text{mS/cm}^2$, $g_L = 2\text{mS/cm}^2$, $g_{Ca} = 4.4\text{mS/cm}^2$, $v_3 = 12\text{mV}$, $v_4 = 17.4\text{mV}$, and $\phi = \frac{1}{15}\text{ms}^{-1}$. The dynamical behavior of (46) with $\hat{\mu} = 0$ has been well studied for $I_{\text{ext}} = 0$, with the current $I_{\text{bias}} =$ constant often playing the role of the bifurcation parameter. For that case there is a SNIC (saddle node on an invariant circle) bifurcation [35] at $I_{\text{bias}} = I_c \approx 44.09\mu\text{A/cm}^2$, and corresponding voltage $v = v_c \approx -27.14\text{mV}$, so that for $I_{\text{bias}} < I_c$, there exists a stable equilibrium and unstable equilibria. For $I_{\text{bias}} > I_c$, the system exhibits oscillations whose frequency increases from zero with $I_{\text{bias}} - I_c$, and there is a Hopf bifurcation for I_{bias} above $60\mu\text{A/cm}^2$, which we do not consider here. The dynamics of an ML-type neuron with periodic external input and constant I_{bias} has been studied in [36, 37].

We focus on transitions from the stable steady state to oscillations for a current that is slowly increasing with rate $\hat{\mu} \ll 1$, modeled here as slowly varying I_{bias} for simplicity but alternatively it could be an input current, and a periodic forcing $I_{\text{ext}} = \hat{A}\sin(\hat{\Omega}t)$. Sample trajectories superimposed on the static bifurcation structure are shown in Figure 10. To determine the tipping points, that is, the value of I_{bias} for the transition, we transform (46) to a form similar to the canonical model (1), rescaling time $\hat{t} = \gamma t$ and normalizing the system about the bifurcation point (v_c, I_c):

$$
\begin{aligned}
\frac{\mathrm{d}x}{\mathrm{d}t} &= h(x) - g_K(x+\mathcal{D})w + b(t) + A\sin(\Omega t)\\
&= b(t) - g_{Ca}m_\infty(x)\left(x + 1 - \frac{v_{Ca}}{v_c}\right) - g_L\left(x + 1 - \frac{v_L}{v_c}\right) + \frac{I_c}{v_c}\\
&\quad - g_K\left(x + 1 - \frac{v_K}{v_c}\right)w + A\sin(\Omega t),\\
\frac{\mathrm{d}w}{\mathrm{d}t} &= \kappa(x)(w_\infty(x) - w), \qquad \kappa(x) = \gamma\hat{\kappa}(v_c(x+1)), \qquad w_\infty(x) = \hat{w}_\infty(v_c(x+1)),\\
\frac{\mathrm{d}b}{\mathrm{d}t} &= -\mu = -\frac{\gamma}{|v_c|}\hat{\mu},\\
x &= \frac{v - v_c}{v_c}, \quad b = \frac{I_{\text{bias}} - I_c}{v_c}, \quad \Omega = \gamma\hat{\Omega}_c, \quad v_cA = \hat{A}, \quad m_\infty(x) = \hat{m}_\infty(v_c(x+1))\,.
\end{aligned}
\tag{47}
$$

For $\mu = 0$ and $A = 0$, the bifurcation point (b_c, x_c) is at the origin for the transformed system (47). Figure 10 shows the bifurcation diagram for (46) and (47), with trajectories for $A = 0$ and $A \neq 0$ obtained from the corresponding systems with $\mu \neq 0$. We note here that for the transformed system, the bifurcation parameter b and dependent variable x take $O(1)$ values. For the system in this form, it is then straightforward to identify different scales related to slow drift, high and low frequency, or large amplitude. Such an identification is important in choosing the correct approach to approximate the tipping point.

Before considering the case with $A \neq 0$, we give an analytical expression for the tipping point without oscillatory forcing $A = 0$, which is compared below with the tipping point for $A \neq 0$. It is useful to find the tipping point for the generic system of the form

$$
\frac{dx}{dt} = Da + k_0 + k_1x + k_2x^2\,, \quad \frac{da}{dt} = -\mu\,.
\tag{48}
$$

Applying the scaling of [9] described in section 2, completing the square in (48), and using

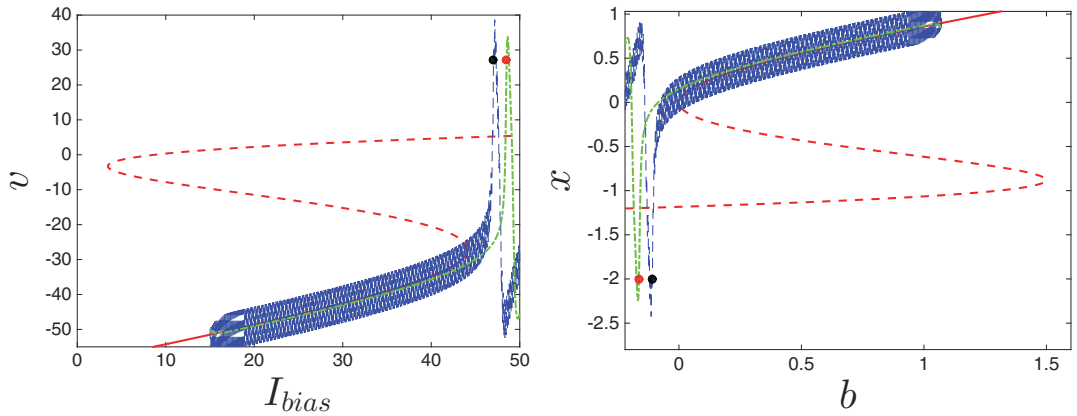

Figure 10. *Left: The bifurcation diagrams of (46) indicating the stable (red solid line) and unstable (red dashed line) branches. The trajectories for $\hat{A} = 0$ (green dash-dotted line) and $\hat{A} \neq 0$ (blue dashed line) are superimposed on these curves, with the corresponding tipping points indicated by solid circles. Note that tipping occurs for a smaller value of $I_{\rm bias}$ for the case $\hat{A} \neq 0$. Right: Same as left panel, but for the transformed system (47).*

a straightforward transformation again yields an Airy equation, from which we obtain the singularity corresponding to the tipping point for (48),

$$a_g = (D|k_2|)^{-1/3} a_d - \frac{a_s}{D} \qquad \text{for} \quad a_s = k_0 + \frac{k_1^2}{4|k_2|}, \tag{49}$$

where a_d is the tipping point in (4) for the symmetric case and a_s gives the shift for a general quadratic polynomial in (48), in contrast to the symmetric case.

For $A = 0$ in (47) we obtain an approximation to the tipping point using a local expansion about $x = 0$. Noting that $0 < \kappa(0) = O(1)$ we expect w to relax to w_∞, so that the local approximation for (47) is

$$\begin{aligned} \frac{dx}{dt} &\approx b + h_0^0 + h_1^0 x + h_2^0 x^2 - g_K(x + \mathcal{D})[w_\infty(0) + w'_\infty(0)x + w''_\infty(0)x^2/2], \\ \frac{db}{dt} &= -\mu, \qquad h_j^0 = j! h^{(j)}(x)|_{x=0}\,. \end{aligned} \tag{50}$$

Then the approximate tipping point for $A = 0$ is given by (49) with $D = 1$ and

$$k_0 = h_0^0 - g_K \mathcal{D} w_\infty(0), \quad k_1 = h_1^0 - g_K(w_\infty(0) + \mathcal{D} w'_\infty(0)), \quad k_2 = h_2^0 - g_K\left(w'_\infty(0) + \mathcal{D}\frac{w''_\infty(0)}{2}\right). \tag{51}$$

Note that $k_0 = k_1 = 0$ in (51) following from the quadratic form for the saddle node bifurcation at $b = 0$ and $x = 0$, so that the resulting tipping point for (50) is $b_{ml} = |k_2|^{-1/3} a_d$.

5.1. High frequency oscillation $\Omega \gg 1$. We use the approach of section 3.2 to study the case $\mu \ll 1$ and $\Omega \gg 1$ in (47), again writing $\Omega = \mu^{-\lambda}$. We restrict our attention to the case where $A = O(1)$.

We introduce the fast time scale $T = \mu^\lambda t$ and the slow time scale $\tau = \mu t$ and substitute the multiple scale approximations for x and w,

$$x \sim x_0(T,\tau) + \mu^\lambda x_1(T,\tau) + \cdots , \tag{52}$$

$$w \sim w_0(T,\tau) + \mu^\lambda w_1(T,\tau) + \cdots , \tag{53}$$

into (47), yielding the sequence of equations

$$\begin{aligned} O(1) &: x_{0T} = w_{0T} = 0, \Rightarrow x_0 = x_0(\tau), w_0 = w_0(\tau), \\ O(\mu^\lambda) &: x_{1T} = b + h(x_0) - g_k(x_0 + D)w_0 + A\sin(T), \end{aligned} \tag{54}$$

$$w_{1T} = \kappa(x_0)(w_\infty(x_0) - w_0)\,. \tag{55}$$

We apply a solvability condition similar to (9), namely, that the inner product of the right-hand side of (55) with the homogeneous solutions (x and w constant with respect to T) vanishes. This yields

$$\begin{aligned} &\lim_{L\to\infty} \frac{1}{L}\int_0^L [b + h(x_0) - g_K(x_0 + \mathcal{D})w_0 + A\sin(T)]\; dT = 0, \\ &\lim_{L\to\infty} \frac{1}{L}\int_0^L \kappa(x_0)(w_\infty(x_0) - w_0)\, dT = 0\,. \end{aligned} \tag{56}$$

Then the asymptotic approximation of x for $b(\tau) = O(1)$ is

$$\begin{aligned} &x \sim x_0 + \mu^\lambda[-A\cos(T)] + \cdots , \quad \text{where} \quad -b = h(x_0) - g_K(x_0 + \mathcal{D})w_\infty(x_0), \\ &w \sim w_\infty(x_0) + \cdots , \end{aligned} \tag{57}$$

where x_0 in (57) is the stable equilibrium of (47), shown as the solid curve in Figure 10 (right). The asymptotic approximation describes the attracting solution of (47) away from $b = 0$, but does not give the tipping point.

To determine the location of the tipping point, we use a local approximation for $x \ll 1$ similar to that used in section 3.2,

$$\begin{aligned} &x = \mathcal{X}(T) + z(T,s), \qquad \mathcal{X}(T) = -\Omega^{-1}A\cos(T), \\ &w = W_0(T,s) + \Omega^{-1}W_1(T,s), \end{aligned} \tag{58}$$

$$z = z_0(T,s) + \Omega^{-1}z_1(T,s), \qquad s = \mu^{1/3}t\,, \tag{59}$$

that is, the solution is given by oscillations on the T scale plus a correction z. We could introduce additional scalings of $z = O(\mu^{1/3})$ and $b = O(\mu^{2/3})$ as in (3.2), but as it does not affect the result, we use z and b for simplicity. We also introduce quadratic polynomials given by Taylor expansions of $h(x)$, $\kappa(x)$, and $w_\infty(x)$ about $x = 0$, facilitating explicit expressions for the tipping point. Then substituting (58)–(59) into (47), we find that W_{0T} and z_{0T} vanish, so that $W_0 = W_0(s)$, $z_0 = z_0(s)$. Approximations for W_0 and z_0 are obtained at the next order, analogous to (20) as shown in Appendix D. We apply the solvability condition as in (56) to the equations for W_1 and z_1, yielding for W_0

$$W_0 \sim w_\infty(0) + W_{00} + W_{01}z_0 + W_{02}z_0^2\,, \tag{60}$$

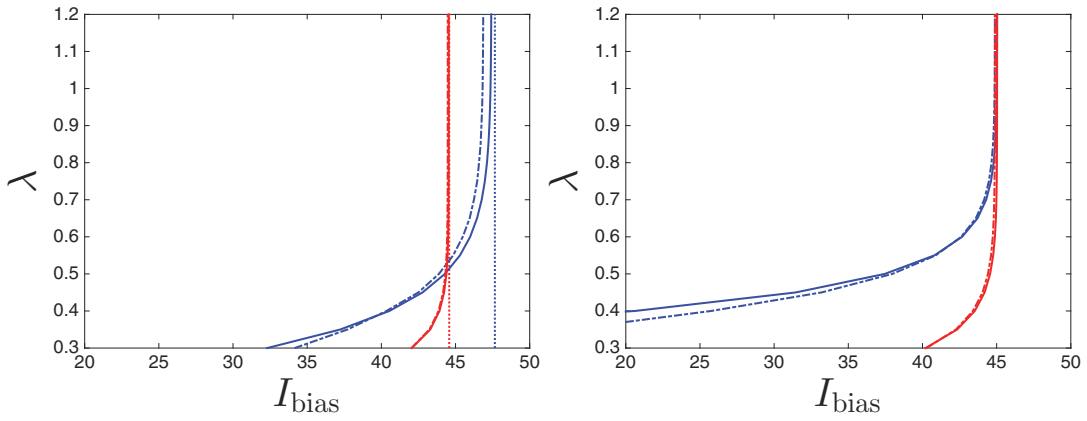

Figure 11. *The value I_{bias} corresponding to tipping in (46) vs. λ for $\Omega = \mu^{-\lambda}$. The asymptotic results obtained from (62) (solid lines) are compared with numerical simulations (dash-dotted lines) obtained using the condition for tipping as $v = |v_c|$ in (46). Left: Results are shown for amplitude $A = 2$ ($\hat{A} = -54.275$) and two drifting rates $\mu = 0.001$ ($\hat{\mu} = 0.0014$) (red) and $\mu = 0.02$ ($\hat{\mu} = 0.0271$) (blue) with asymptotes for large Ω approximated by (51) (vertical dotted lines) as $I_{\text{bias}} = 44.58$ and $I_{\text{bias}} = 47.65$, respectively. Right: Results are shown for $\mu = 0.003$ ($\hat{\mu} = 0.0041$) and amplitude values $A = 2$ (red) and $A = 8$ ($\hat{A} = 217.10$) (blue), with earlier tipping for larger ratios A/Ω.*

with the coefficients W_{00}, W_{01}, and W_{02} given in (116). Then the equation for z_0 written in terms of t is

$$z_{0t} = b + h_0^0 + h_1^0 z_0 + h_2^0 z_0^2 + h_2^0 \frac{A^2}{2\Omega^2} - g_K(z_0 + \mathcal{D})W_0. \tag{61}$$

Applying (48)–(49) yields the singularity for (61)

$$b_{hf} = |h_2^{\text{hf}}|^{-1/3} a_d - b_s \quad \text{for} \quad b_s = h_0^{\text{hf}} + \frac{(h_1^{\text{hf}})^2}{4|h_2^{\text{hf}}|}, \quad \text{where} \tag{62}$$

$$h_0^{\text{hf}} = -g_k \mathcal{D} W_{00} + h_2^0 \frac{A^2}{2\Omega^2}, \qquad h_1^{\text{hf}} = -g_K(W_{00} + \mathcal{D}(W_{01} - w'_\infty(0))),$$
$$h_2^{\text{hf}} = h_2^0 - g_K(W_{01} + \mathcal{D}W_{02}),$$

where we have used the fact that k_0 and k_1 in (51) vanish. Note that for $\Omega \gg 1$, $W_{01} - w'_\infty(0)$ and W_{00} are proportional to Ω^{-2}, as are h_0^{hf} and h_1^{hf}. Then we recover (51) as $\Omega^{-2} \to 0$.

In Figure 11 we compare the asymptotic approximation for the tipping point for I_{bias} obtained from (62) as a function of the exponent λ for $\Omega = \mu^{-\lambda}$ with numerical simulations for different drifting rates μ and amplitudes A. For larger values of the ratio A/Ω we see an increased advance of the tipping point. For larger λ corresponding to higher frequencies Ω, the delay effect caused by slowly varying drifting rate $\hat{\mu}$ dominates the location of the tipping point, regardless of the amplitude of the oscillatory forcing. For smaller λ, larger amplitude $\hat{A}$ triggers earlier tipping.

We note the importance of deriving these results within the framework of the transformed system (47) for x. Figure 11 shows good agreement of the asymptotic and computational results for $\Omega = \mu^{\lambda}$ over the range $\lambda > 0.3$, as predicted by the asymptotic results for the

canonical model. Considering the variables of the original ML system (46), we see that $\hat{\Omega}$ is smaller than Ω by a factor of $\gamma = 20$, while $\hat{\mu} \approx 1.36\mu$. Applying the asymptotic analysis in the original variables could suggest that good approximations are available over a smaller range of parameter values and could lead to the use of an expansion that is not appropriate for the dynamics.

5.2. Low frequency oscillation $\Omega \ll 1$. As in section 4, we write $\Omega = \mathcal{C}\mu$, rescale time as $\tau = \mu t$ and write x and w as functions of $b(\tau) = b_0 - \tau$. Then (47) becomes

$$-\mu \frac{\mathrm{d}x}{\mathrm{d}b} = b + h(x) - g_K(x + \mathcal{D})w + A\sin(\mathcal{C}(b_0 - b)), \tag{63}$$

$$-\mu \frac{\mathrm{d}w}{\mathrm{d}b} = \kappa(x)(w_\infty(x) - w)\,. \tag{64}$$

Substituting the asymptotic expansion (53), we find the leading order approximation of $w(x)$ is $w_0 = w_\infty(x_0)$ for $x_0 \sim O(1)$ and for x_0

$$b + h(x_0) - g_K(x_0 + \mathcal{D})w_\infty(x_0) + A\sin(\mathcal{C}(b_0 - b)) \equiv \Phi(x_0, b) = 0\,. \tag{65}$$

As in section 4, we expect the tipping to occur in the region where the outer approximation is not valid, for a pair (b_r, x_r). A Taylor expansion of Φ about x_r evaluated at b_r, keeping up to quadratic terms, yields

$$x_0 - x_r = -\frac{1}{2\Phi_2^r}\left[\Phi_1^r \pm \sqrt{(\Phi_1^r)^2 - 4\Phi_2^r \cdot \mathcal{F}(b_r)}\right], \qquad \Phi_j^r = j!\frac{\partial^j \Phi}{\partial x^j}(x_r, b_r), \qquad \mathcal{F}(b_r) = \Phi_0^r\,, \tag{66}$$

where the positive sign corresponds to the solution that is attracting. It follows that the approximation for x_0 is no longer valid for $b < b_r$, where $4\mathcal{F}(b_r) = (\Phi_1^r)^2/\Phi_2^r$ and $2(x_0 - x_r) = -\Phi_1^r/\Phi_2^r$. As $x_0 \to x_r$, $\Phi_1^r \to 0$, from which we conclude that $x_r = x_c = 0$, the value of x at the saddle node bifurcation for the static case. As a result we expect that tipping occurs near $b = b_r$ and $x = 0$. Note that $\mathcal{F}(b)$ then has the same functional form as $f(a)$ in (26).

As in section 4 we use a local analysis in terms of $b - b_r = \mu^{2/3}\mathcal{B}$ and $x = \mu^{1/3}\chi$ applied to (63), yielding

$$-\mu^{2/3}\chi_{\mathcal{B}} = \mathcal{F}'(b_r)\mu^{2/3}\mathcal{B} + k_2(\mu^{1/3}\chi)^2 + o(\mu^{2/3}), \tag{67}$$

where $\mathcal{F}'(b_r) = 1 - \mathcal{C}A\cos(\mathcal{C}(b_0 - b_r))$ and k_2 is given in (51). Then using the result (49) yields the tipping point

$$b_{\mathrm{lf}} = b_r + \frac{a_d}{(\mathcal{F}'(b_r)|k_2|)^{1/3}}\,. \tag{68}$$

The result for b_{lf} relies on $\mathcal{F}'(b_r) = O(1)$, and as in section 4, if $\mathcal{F}'(b)$ vanishes, the approximation (67) is not valid. Near a value $b = b_m$, where $\mathcal{F}(b_m) = \mathcal{F}'(b_m) = 0$, we again expect to find a jump in the location of the tipping point as a function of amplitude for a critical value $A = A_c$. Following the analysis of section 4, we provide a local analysis for (b, A) close to (b_m, A_m), which satisfy the conditions

$$\mathcal{F}(b_m) = b_m + A\sin(\mathcal{C}(b_0 - b_m)) = 0, \tag{69}$$

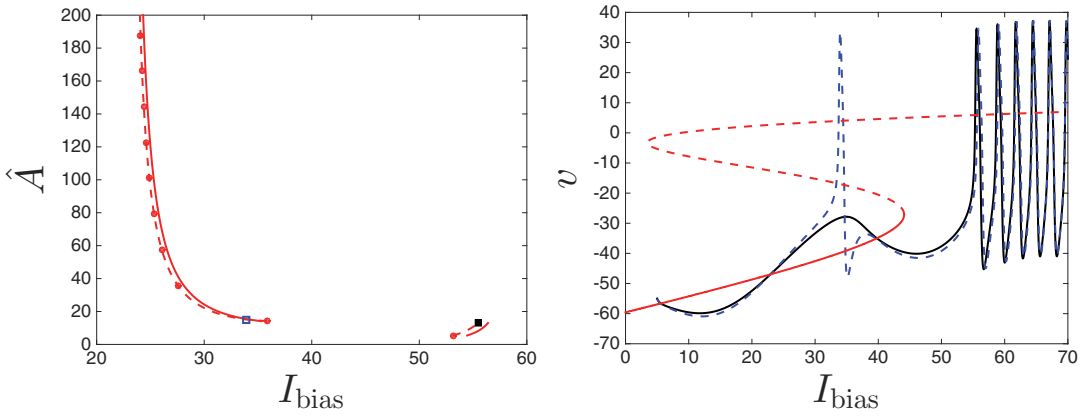

Figure 12. *Results are shown for $\mu = 0.04$, $\Omega = 0.2$. Left: The location of the tipping points obtained by numerical simulations of (46) (red dashed line with dots) as a function of amplitude $\hat{A}$, compared with the asymptotic approximation given by (68) (red solid line), with tipping defined as $v = |v_c|$. Right: Numerical simulations for different amplitudes $\hat{A}$, $-\hat{A} \approx 13.02$ (black solid line) and $-\hat{A} \approx 15.20$ (blue dashed line). The related tipping points are shown as the black solid square and blue open square in the left panel.*

$$\mathcal{F}'(b_m) = 1 - \mathcal{C}A_m \cos(\mathcal{C}(b_0 - b_m)) = 0, \Rightarrow 1 + \mathcal{C}^2 b_m^2 = \mathcal{C}^2 A_m^2 . \tag{70}$$

To find $A_c > A_m$ for which there is a jump in the location of the tipping point, we consider the concavity of x in (63) with respect to b near b_m. Substituting local variables

$$b - b_m = \mu\eta, \qquad x = \mu\xi, \qquad \text{and } A = A_m + \mu A_1, \tag{71}$$

into (63) and (64), we find the leading contributions to $x'(b)$ and $x''(b)$ in terms of the local variables,

$$\frac{\mathrm{d}^2\xi}{\mathrm{d}\eta^2} = \mu\frac{A_1}{\mathcal{C}A_m} - \mu(\mathcal{C}^2\eta b_m) - \mu k_2 \xi \frac{2A_1 b_m}{A_m} + O(\mu^2), \tag{72}$$

$$\frac{\mathrm{d}\xi}{\mathrm{d}\eta} = \frac{b_m A_1}{A_m} + O(\mu) \tag{73}$$

for k_2 from (51). From (72) we see that the line corresponding to the concavity threshold, across which the trajectory of x changes its concavity, is given by

$$\xi_c^{\mathrm{ML}} = -\frac{\mathcal{C}^2 A_m}{2k_2 A_1}\eta + \frac{1}{2\mathcal{C}k_2 b_m} . \tag{74}$$

We compare the slope of (74) to the slope of x from (73), as in (35)–(37). Where these two slopes are equal, we find the change in concavity of the trajectory that corresponds to tipping. Setting the slope of (74) equal to (73) and solving for A_1 yields

$$A_1 = \frac{\mathcal{C}A_m}{\sqrt{2|k_2|b_m}} \qquad \Rightarrow \qquad A_c = A_m + \frac{\Omega A_m}{\sqrt{2|k_2|b_m}}. \tag{75}$$

Figure 12 (left) compares the asymptotic approximation of the location of the tipping points given by (68) and (75) to the results from numerical simulations. We show the tipping

point as a function of the amplitude $\hat{A}$, with the jump in this curve occurring at the amplitude threshold A_c given by (75). Figure 12 (right) illustrates the character of the early transition near $A = A_c$ for (46) with early tipping occurring for $A > A_c$ but not for $A < A_c$. For the value of I_{bias} where early tipping occurs, there is not an attracting oscillatory solution nearby, so following the tipping event, the system does not remain in the oscillatory state. This behavior is in contrast to the system (1), for which the tipping is irreversible. For some combinations of b_0 and A, the tipping point for (47) associated with A_c is closer to the SNIC bifurcation, in which case after the tipping for $A > A_c$ the system remains in the oscillatory state.

6. Energy balance model for sea ice. We apply the analysis to an energy balance model developed by Eisenman and Wettlaufer [11], as mentioned in the introduction. The model describes sea ice dynamics in terms of the change of the energy per unit area, stored either as latent heat in sea ice or as sensible heat in the ocean mixed layer,

$$E \equiv \begin{cases} -L_i h_i, & E < 0, \\ c_{\text{ml}} H_{\text{ml}} T_{\text{ml}}, & E \geq 0, \end{cases} \tag{76}$$

where L_i is the latent heat of fusion for sea ice, h_i is the thickness of sea ice, c_{ml} is the heat capacity of the ocean mixed layer, H_{ml} is the depth of the mixed layer, and T_{ml} is the temperature difference from the freezing point 0°C. The reduced system, derived from the full heat conduction equations for sea ice thermodynamics of [29], expresses the energy dynamics in terms of sensible and latent heat fluxes, outgoing longwave and incoming shortwave radiative surface fluxes. We focus on the partially linearized version model of [11] that neglects ice export which has the form

$$\frac{\mathrm{d}E}{\mathrm{d}t} = [1 - \alpha(E)]F_S(t) - F_0(t) + \Delta F_0 - F_T(t)T(t, E) + F_B. \tag{77}$$

Here $F_S(t)$ describes the shortwave radiation flux which is seasonally varying, with $[1 - \alpha(E)]F_S(t)$ describing surface shortwave radiation related to albedo feedback,

$$\alpha(E) = \frac{\alpha_{\text{ml}} + \alpha_i}{2} + \frac{\alpha_{\text{ml}} - \alpha_i}{2} \tanh\left(\frac{E}{L_i h_\alpha}\right), \tag{78}$$

where α_{ml} and α_i are constants for albedo feedback for the mixed layer and surface ice, respectively. The factor h_α is an ice thickness range for smooth transition from α_i to α_{ml}. The temperature dependence of the surface flux is obtained via a linearization of the Stefan–Boltzmann equation, resulting in the outgoing longwave radiation contributions $F_0(t)+F_T(t)T(t, E)$, with the seasonal variation in $F_0(t)$ and $F_T(t)$ determined from combined modeling and observational data (see SI Appendix of [11] for details). The partial linearization given in [11] follows from taking the surface temperature $T(t, E)$ as

$$T(t, E) = \frac{E}{c_{\text{ml}} H_{\text{ml}}}. \tag{79}$$

The term F_B describes the heat flux into the bottom of the sea ice or the ocean mixed layer. The additional contribution ΔF_0 captures a change in the surface heat flux, representing warming in the model for $\Delta F_0 > 0$.

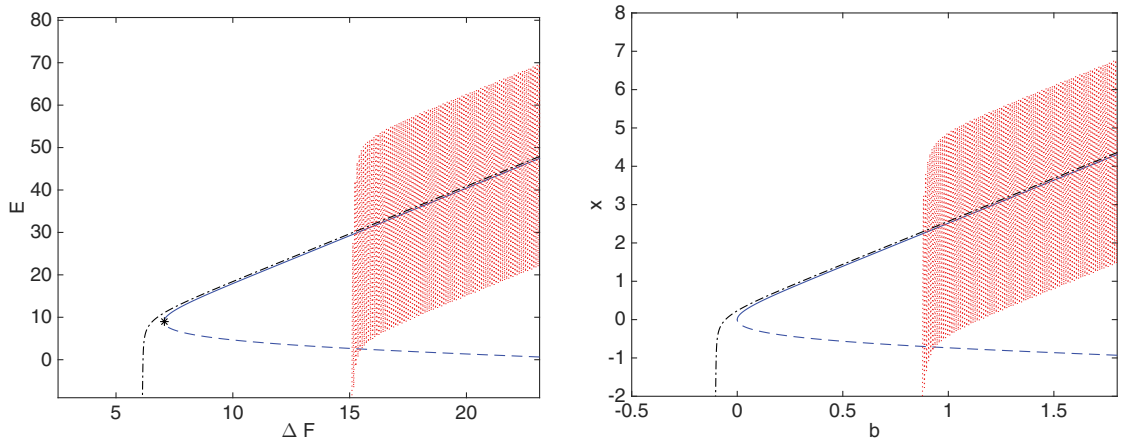

Figure 13. *Time series in both panels are shown for $\mu = 0.01$. Left: Time series for E in (81) with oscillatory forcing term g_j (red dotted line) and without, that is, where the oscillatory terms g_j are replaced by their averages G_j (black dash-dotted line). The critical value $(\Delta F_{0c}, E_c)$ is marked with *. The solid (dashed) blue curve corresponds to a stable (unstable) branch of $dE/dt = 0$ in (81) for the averaged model. Right: Time series for x given in (82) with oscillatory forcing term g_j (red dotted line) and without, that is, where the oscillatory terms g_j (black dash-dotted line) are replaced by their averages G_j. The solid (dashed) blue curve corresponds to the stable (unstable) branch of $b = -H(x)$ in (82). When rescaled using the transformation (80), the oscillations for the x approximation are slightly smaller than those for the full E equation, although the difference is negligible on this scale.*

In [11] the nonlinear threshold behavior of the energy was studied through the bifurcation structure of (77) with the seasonally varying terms $F_0(t)$, $F_S(t)$, and $F_T(t)$. Attracting periodic states for fixed ΔF_0 were determined by simulating the equation, allowing the system to reach the attracting state, and recording the minimum and maximum value of E for the particular value of ΔF_0. For the parameters in [11], there are two branches of attracting states for $E > 0$ and $E < 0$ in terms of ΔF_0, the bifurcation parameter describing the change to the surface heat flux. These states are bistable for a range of ΔF_0, with each branch losing stability to the other via a saddle node bifurcation. Figure 13 shows the branch corresponding to the stable steady state of the averaged version of (77), that is, with the seasonally varying terms $F_0(t)$, $F_S(t)$, and $F_T(t)$ replaced by their averages, and for $E \geq 0$ and ΔF_0 a positive constant. We denote the saddle node bifurcation value on this branch as $(\Delta F_{0c}, E_c)$ and also show the unstable branch for that system. As would be expected from the analysis of previous sections, the saddle node bifurcation for the averaged system differs considerably from the tipping point when there is large amplitude periodic forcing. The parameters values are as in [11]: $L_i = 9.4\ \mathrm{Wm}^{-3}\mathrm{yr}$, $c_{\mathrm{ml}}H_{\mathrm{ml}} = 9.4\mathrm{Wm}^{-2}\mathrm{yrK}^{-1}$, $\alpha_i = 0.68$, $\alpha_{\mathrm{ml}} = 0.2$, $F_B = 2\mathrm{Wm}^{-2}$, and $h_\alpha = 0.5\mathrm{m}$. The seasonally varying quantities take values in the ranges $130\ \mathrm{Wm}^{-2} > F_0(t) > 54\ \mathrm{Wm}^{-2}$, $3.3\ \mathrm{Wm}^{-2}\mathrm{K}^{-1} > F_T(t) > 2.5\ \mathrm{Wm}^{-2}\mathrm{K}^{-1}$, and $310\ \mathrm{Wm}^{-2} > F_S(t) > 0\ \mathrm{Wm}^{-2}$.

In considering the case where the surface heat flux varies slowly over time with a rate $\tilde{\mu}$, we use the asymptotic approaches described in previous sections to study tipping from the attracting branch $E \geq 0$, noting that by symmetry a similar approach applies for the other branch $E < 0$. We contrast the location of the tipping point for the averaged model with the tipping location in the case where the oscillatory functions $F_0(t)$, $F_S(t)$, and $F_T(t)$ are not

replaced with their averages. Since we obtain analytical expressions for the tipping point, we can easily explore the parametric dependence on the location of the tipping point, which has implications for the bifurcation structure as a function of the parameters. We note that the computational approach used in [11] to explore bifurcations corresponds to the limit $\tilde{\mu} \to 0$.

The fluctuations in $F_0(t)$, $F_S(t)$, and $F_T(t)$ are given as a series of monthly measurements [11, SI Appendix], which we interpolate and approximate using a (finite) Fourier series approximation. We assume that the fluctuations are the same year to year. To allow easy identification of the oscillatory forcing terms, we write (77) in a form analogous to that of (1) and shift the bifurcation point for the averaged system from $(\Delta F_{0c}, E_c)$ to the origin, as shown in Figure 13. We rescale the system appropriately, so that the resulting dependent variable x and corresponding slowly varying parameter b are $O(1)$ quantities. Substituting

$$x = \frac{E - E_c}{E_c}, \quad b = \frac{\Delta F_0 - \Delta F_{0c}}{E_c} \tag{80}$$

into (77), and taking ΔF_0 to vary slowly in time with rate $\tilde{\mu}$, yields

$$\begin{aligned} \frac{\mathrm{d}x}{\mathrm{d}t} &= g_1(t) + g_2(t)\tanh(g_3(x+1)) + g_4(t)x + b, \\ \frac{\mathrm{d}b}{\mathrm{d}t} &= -\mu = -\tilde{\mu}/E_c. \end{aligned} \tag{81}$$

$$g_1(t) = E_c^{-1}\left[\left(1 - \frac{\alpha_{\mathrm{ml}} + \alpha_i}{2}\right) F_S(t) - F_0(t) + F_B\right] + \frac{\Delta F_{0c}}{E_c} + g_4(t),$$

$$g_2(t) = -\frac{\alpha_{\mathrm{ml}} - \alpha_i}{2E_c} F_S(t), \qquad g_3 = \frac{1}{L_i h_\alpha} E_c, \qquad g_4(t) = -\frac{F_T(t)}{c_{\mathrm{ml}} H_{\mathrm{ml}}}.$$

In contrast to (1), which has only additive periodic forcing, (81) has both multiplicative oscillatory forcing terms with coefficients $g_2(t)$ and $g_4(t)$ and an additive oscillatory term $g_1(t)$. So we consider approximations for the terms involving g_2 and g_4 that replace the multiplicative oscillations with reasonable additive oscillations. The oscillations in g_1 have an amplitude of ≈ 20, $g_2(t)$ has an amplitude of ≈ 5, while $g_4(t)$ has oscillations with relatively small amplitude of ≈ 0.5. We anticipate that the fluctuations of $g_4(t)$, as compared with those of $g_1(t)$ and $g_2(t)$, have a negligible effect on tipping, generally occurring for $x = O(1)$ or smaller. So we neglect the oscillations in the term $g_4(t)x$ by replacing $g_4(t)$ with its average. Furthermore the results from the previous sections suggest that large oscillations in g_1 drive tipping for $O(1)$ values of the bifurcation parameter b and thus for $O(1)$ values of x, for which $\tanh(g_3(x+1)) \approx 1$. Then it is reasonable to approximate $g_2(t)\tanh(g_3(x+1)) \approx G_2\tanh(g_3(x+1)) + g_2(t) - G_2$, so that (81) is approximated by

$$\begin{aligned} \frac{\mathrm{d}x}{\mathrm{d}t} &= b + H(x) + q(T), \\ \frac{\mathrm{d}b}{\mathrm{d}t} &= -\mu. \end{aligned} \tag{82}$$

$$H(x) = G_1 + G_2\tanh(g_3(x+1)) + G_4 x, \quad q(T) = g_1(t) - G_1 + g_2(t) - G_2\,, \tag{83}$$

where G_j is the average value of $g_j(t)$ over one period for $j = 1, 2, 4$ and $q(T)$ is an oscillatory function with mean zero and period of $t = 1$. With the oscillatory contributions represented

as a Fourier series, the time scale of $q(T)$ is $T = \Omega t$ with $\Omega = 6.28$. The computed trajectories shown in Figure 13 illustrate the validity of (82) as an approximation for (81).

We note here that for the transformed system, as in section 5, the bifurcation parameter b and dependent variable x take $O(1)$ values. Then we identify different scales related to slow drift, high and low frequency, or large amplitude in this setting, which again is important in choosing the appropriate asymptotic approach.

An analytical expression for the tipping point in the case $q(T) = 0$ is found as described in (48)–(49), based on a Taylor series of $H(x)$ in (82) about $x = 0$. Then

$$b_d = |H_2|^{-1/3} a_d - b_p \quad \text{for} \quad b_p = H_0 + \frac{H_1^2}{4|H_2|}, \qquad H_j = j! H^{(j)}(0)$$

is the tipping point for (82) for $q(T) = 0$ and is compared below with the tipping point for $q(T) \neq 0$. We note that H_0 and H_1 are small, but not identically zero, as are the analogous terms in section 5, since we are using an approximate system (82) rather than the full model from which the saddle node bifurcation point $(\Delta F_{0c}, E_c)$ was determined.

Next, we consider whether (82) corresponds to high frequency forcing as in section 3.2 or low frequency forcing as in section 4. For $\mu \ll 1$ and $\Omega = 6.28$, we would expect this system to be in the high frequency case. However, since the amplitude of the oscillations is large, section 3.3 indicates that $\log(A)/\log(\Omega)$ must be considered to determine whether oscillations with amplitude A correspond to high or low frequency forcing in a rescaled system. We find that $4/3 < \log(\max(q(T)))/\log(\Omega) < 2$ for (82) falls in between the asymptotic ranges identified in section 3.3 for the high and low frequency cases. Nevertheless, we adapt the concepts from the previous sections to approximate the shift in the tipping point driven by the oscillations in (82).

We begin with an outer approximation for x based on the approach from section 3.2 and Appendix B. Substituting a multiple scale approximation, $x(\mu t, T) = x_0(\mu t, T) + \Omega^{-1} x_1(\mu t, T) + \cdots$ for $T = \Omega t$ into (82), we get

$$x_{0T} = 0, \Rightarrow x_0 = x_0(t), \quad x_{1T} = b + H(x_0) + q(T)\,. \tag{84}$$

The solvability condition (9) for x_1 yields $b + H(x_0) = 0$ so that the leading order contributions to x are

$$x \sim H_+^{-1}(-b) + \Omega^{-1} Q(T)\,, \quad Q'(T) = q(T), \tag{85}$$

where $H_+^{-1}(-b) > 0$ corresponds to the stable branch for $x > 0$ and $Q(T)$ has zero average. The leading order approximation for the outer solution (85) is composed of oscillations $\Omega^{-1} Q(T)$ about the branch of the averaged system $b = -H(x)$.

Where the outer approximation is no longer valid, we construct a local expansion. To find an appropriate local approximation, we appeal to the results shown for the canonical model in section 3.2, noting that we must adapt that approach since the amplitude of the oscillatory forcing is large. If the amplitude was $O(1)$, we would write the inner solution in the multiple scale form $x = \Omega^{-1} Q(T) + Y(t, T)$ analogous to the local expansion in section 3.2. This form is an approximation composed of oscillations near $x = 0$ with Y a small correction to be determined. However, since the oscillations are large for this application, we expect

that the outer approximation breaks down away from $x = 0$. In fact, if we examine the outer approximation (85), we see that it reaches values of x that are on the unstable lower branch shown in Figure 13. We can approximate the value of x where this occurs by identifying a value b^* and corresponding $x^* = H_+^{-1}(-b^*)$ on the stable branch of $b = -H(x)$, where

$$H_+^{-1}(-b^*) + \Omega^{-1} \min(Q(T)) = H_-^{-1}(-b^*)\,, \tag{86}$$

where $H_-^{-1}(-b^*)$ is on the unstable branch shown in Figure 13. Then we adapt the approach from section 3.2 writing the solution in the multiple scale form that has oscillations about x^* with Y a correction,

$$x = x^* + \Omega^{-1}Q(T) + Y(T,t). \tag{87}$$

We could also rescale b, Y, and the time scale t with a power of μ. However, we obtain the same result without this rescaling, so for simplicity we do not introduce such rescaled variables here. Substituting the multiple scale expression (87) into (82) yields

$$\Omega Y_T = -Y_t + b + H(x^* + \Omega^{-1}Q + Y) \tag{88}$$

$$\sim -Y_t + b + H(x^* + \Omega^{-1}Q) + H'(x^* + \Omega^{-1}Q)Y + \frac{H''(x^* + \Omega^{-1}Q)}{2}Y^2\,. \tag{89}$$

In contrast to the approximation used in (114) for the ML model or in (48), we have not replaced $H(x)$ with a polynomial in x before substituting (87). The reason that we avoid this step is that the forcing $q(T)$ is relatively large in this case, so we must consider $H(x)$ over a larger range of x values. Over this range, it is not possible to approximate $H(x)$ accurately with a Taylor series about a single value of x. Rather we have substituted (87) directly into $H(x)$ and then expanded about $Y = 0$, assuming that Y is a small correction. Then the solvability condition (9) for (89) yields the equation for Y:

$$\begin{aligned} Y_t = b &+ \left(\lim_{L\to\infty}\frac{1}{L}\int_0^L H(x^* + \Omega^{-1}Q(T))dT\right) + \left(\lim_{L\to\infty}\frac{1}{L}\int_0^L H'(x^* + \Omega^{-1}Q(T))dT\right) Y \\ &+ \left(\lim_{L\to\infty}\frac{1}{L}\int_0^L \frac{H''(x^* + \Omega^{-1}Q(T))}{2}dT\right) Y^2 \\ &= b + \mathcal{H}_0 + \mathcal{H}_1 Y + \mathcal{H}_2 Y^2\,. \end{aligned} \tag{90}$$

From (86) we get $x^* \approx 2.2$. Then we obtain the tipping point from the singularity for (90) using the results from (48) and

$$b_{\text{tip}} = |\mathcal{H}_2|^{-1/3}a_d - b_Q \quad \text{for} \quad b_Q = \mathcal{H}_0 + \frac{\mathcal{H}_1^2}{4|\mathcal{H}_2|}\,. \tag{91}$$

In Figure 14 we compared this approximation with the numerical results in terms of the original variables E and ΔF_0. As would be expected for a system forced by oscillations with a large amplitude-to-frequency ratio, the advance of the tipping point is dominated by the oscillations. As $\tilde{\mu} \to 0$, the tipping point approaches the end of the branch of attracting oscillatory solutions computed in [11].

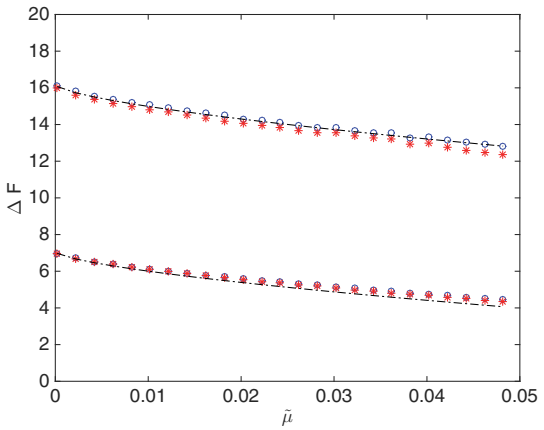

Figure 14. *Comparison of the tipping points ΔF_0 obtained from the asymptotic approximation (91) (black dash-dotted lines) compared with the numerically obtained values from the full model for E (81) (blue o's) and from the approximate model for x (82) (red *'s). The lower values correspond to the tipping point for the averaged system with $g_j(t)$ replaced with G_j, while the upper curve corresponds to the case where the oscillations are not replaced with their averages.*

The fact that we are able to obtain an analytical expression for the tipping point allows us to explore the impact of parameter values on the bifurcation structure of the model and the location of transitions between states. Specifically, we can explore the existence or prominence of hysteresis between different states as a function of the parameters of a periodically forced system. Within the context of a large-scale atmosphere-ocean global climate model studied in [30], the question was considered whether or not parameter variation yields hysteresis in the transitions between states analogous to $E > 0$ and $E < 0$ in (77). There it was seen that the hysteresis obtained for time-varying parameters, predicted by lower dimensional models where there is bistability for different states, is less prominent and in certain contexts it is not observed in the large-scale computations. An analogous question of how the bifurcation structure could change with parameters was explored computationally in [31] for a simplified version of (77). For example, recomputing the bifurcation diagram for different parameter values, [31] shows a loss of bistability with increased contributions to longwave radiation from $F_T(t)$, and thus a loss of the hysteresis loop observed for a varying bifurcation parameter. In the context of tipping, the loss of hysteresis corresponds to shifts in the tipping points so that regions of bistability are no longer observed. The value of the analytical expression for the tipping point (91) is in determining shifts in the tipping location as a function of a parameter, rather than having to recompute the entire bifurcation structure through repeated simulation of the full model over a potentially large range of parameter values.

In Figure 15 we demonstrate how this loss of hysteresis is obtained directly from the analytical expression (91) for the tipping point. The upper right panel shows that increasing the amplitude of $F_T(t)$ causes earlier tipping. For tipping points increased to $\Delta F_0 \approx 31$, there is a loss of hysteresis, since tipping occurs for approximately the same value of ΔF_0 for which there is a transition from the lower solution branch for E (not shown) to the upper branch in Figure 13. The approximation (91), based on (86), indicates this behavior for the amplitude of F_T increased above a factor of about 2.7, as also observed in [31]. For this increase in

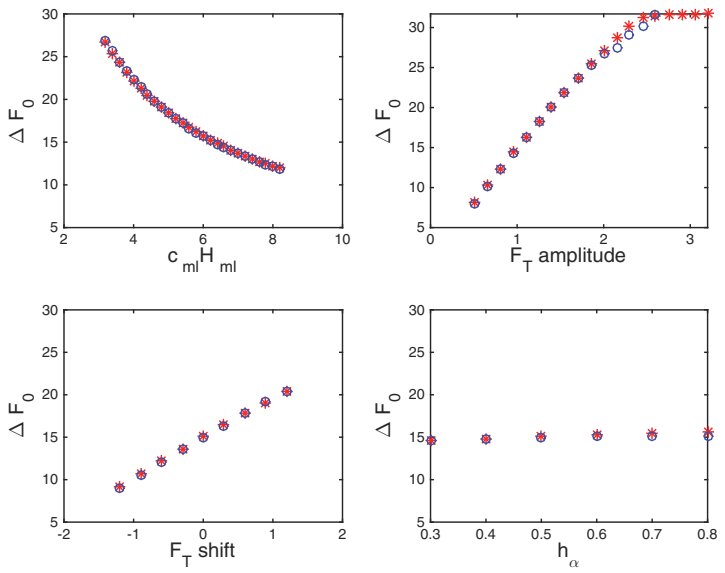

Figure 15. *Analytical approximation (blue o's) and numerical approximation (red *'s) for the value ΔF_0 corresponding to tipping as a function of different parameters: the ratio of E to $T(t,E)$ in (79) (upper left), a multiplicative factor for the amplitude of the oscillations F_T (upper right), a shift in the mean of F_T (lower left), and the ice thickness parameter describing transitions in the albedo (lower right). In the upper right panel, the approximation is not valid for tipping points with values $\Delta F_0 > 31$. This corresponds to larger amplitudes of F_T, for which there is no overlap in the range of ΔF_0 for upper and lower attracting branches of E, indicating no hysteresis for varying ΔF_0. Then determining x^* from (86) is no longer valid for the asymptotic approximation. In that case the numerical approximation asymptotes to $\Delta F_0 \approx 31$.*

the oscillations there is no overlap in b for the upper and lower attracting branches for the solution x, and no intermediate unstable branch. Then determining x^* from (86) is no longer valid, signaling the loss of bistability and of hysteresis. For the same reason, the numerical approximation asymptotes to the value of $\Delta F_0 \approx 31$, as shown in Figure 15 (upper right). From the normalized model (82) we can also identify other parameters $c_{\rm ml}H_{\rm ml}$ and the mean of F_T that can drive a considerable shift in the tipping point. The left panels of Figure 15 show the effect of varying these parameters, which is not as large as for the increased amplitude of F_T, as also observed in [31].

The variation of the tipping point with h_α is also shown. For this model, approximating the tipping location using (86)–(91) is based on the existence of an upper solution branch. Then Figure 15 (lower left) shows the approximation for values h_α, where x^* in (86) can be determined. The upper branch used in (86) no longer exists for h_α sufficiently small, as also seen in [31].

7. Summary and future work. In this paper we have analyzed the factors that determine the location of a tipping point in the canonical model for a saddle node bifurcation with bifurcation parameter a that varies at a slow rate $\mu \ll 1$ and forced by a periodic oscillation with amplitude A and frequency Ω. We see that the main contributions that determine the tipping point location are different for low and high frequencies. In order to get analytical expressions to identify the key factors in the location of the tipping point, we apply the meth-

ods of multiple scales and matched asymptotic expansions to obtain analytical expressions for the combined effect of Ω, A, and μ. The cases of low and high frequencies in the oscillatory forcing naturally require the consideration of different relationships between the time scales of the oscillation and the slow drifting rate. The size of the amplitude also plays an important role.

For a high frequency forcing, there are two competing contributions to the location of the tipping point relative to the static bifurcation point at $a = 0$. The first contribution is a delay due to the slow drifting rate μ of the bifurcation parameter a, well known in a variety of studies without periodic forcing [7, 9]. The second contribution is an advance proportional to the square of the ratio of the amplitude to frequency for the oscillation, observed also in the case where the bifurcation parameter is constant ($\mu = 0$). These contributions reflect that the trajectory in this case is approximated by the linear combination of the slowly varying equilibrium solution found for $A = 0$ in [9] and an additive contribution that takes the form of the oscillatory forcing with a scale factor. Near the tipping point, the trajectory can be expressed in terms of an oscillatory part plus a correction that satisfies an Airy function on the slow time scale, with the oscillations averaged on this time scale shifting the singularity that corresponds to the tipping point. The resulting expressions for these contributions then give an expression for the location of the tipping point that varies continuously with the parameters. Whether the combined effect results in an advance or delay compared to $a = 0$ depends on the magnitude of $\mu^{2/3}$ relative to A^2/Ω^2. In particular, we see noticeable advances of the tipping point for combinations of larger amplitudes with frequencies that are not very large.

Advances in the tipping point due to periodic forcing are even more apparent for lower frequencies. For $\Omega \ll 1$, the trajectory is dominated by a nonlinear combination of the slowly drifting bifurcation parameter and the oscillatory forcing, since they give contributions that are of the same order of magnitude. Then the location of the tipping point depends not only on the amplitude, frequency, and drifting rate, but also on the phase of the oscillation. Tipping occurs near values of a where the trajectory is near $x \sim 0$, where a local analysis reveals that the change of concavity for $x \sim 0$ provides an analytical expression for the tipping point. This expression captures the discontinuous dependence of the tipping location on parameters such as the amplitude. These discontinuities follow directly from the fact that tipping occurs only for values of a where the trajectory is near zero: a slight change in parameters can change the approach to zero of the trajectory, postponing tipping to a later point at which the trajectory crosses zero. This shift in the tipping point is on the order of one period of the low frequency oscillation.

The development of this suite of approaches provides a foundation for capturing the behavior of the tipping point in terms of the key parameters. Within the context of the applications in sections 5 and 6, we have demonstrated how the approximations developed for the canonical model can be used directly in other models. The influence of the oscillations, and thus the choice of the appropriate approximation, depends on certain scaling relationships between drifting rate, amplitude, and frequency. These are identified within the context of the canonical model where the dependent variable and bifurcation parameters take $O(1)$ values and the saddle node bifurcation at the origin. Thus an important step is normalization of the model to this standard form, from which the parameter relationships can be extracted. Within the

transformed model one can already identify parameter ranges where advanced tipping is likely to occur, by relating the results of the canonical model to the rescaled parameters.

The results for both the canonical model and the applications illustrate how the concepts developed within the asymptotic approaches can be extended to wider ranges of parameters. For example, the results of section 4.1 for low frequency, where the frequency is of the same order of magnitude as the drifting rate, are extended in section 4.2 for larger values of frequency that are $O(1)$, by using the values where the regular asymptotic expansion no longer exists as a basis for a local analysis of the change of concavity. Another example of the extension of the method is in the application of section 6, where the ratio of amplitude to frequency for the oscillation is outside of the asymptotic range identified for large amplitude oscillations in section 3.3. Nevertheless, as for the canonical model, we apply a regular or outer expansion, and from conditions where the outer expansion loses its validity we identify the region for a local multiple-scale analysis. The solvability condition for the local approximation again provides an averaged equation with quadratic nonlinearity, whose singularity provides the approximation of the location of the tipping point.

We have also compared the advance of the tipping point for high frequency forcing with the shift due to additive white noise forcing, where a significant advance of the tipping point occurs if the magnitude of the noisy forcing scales as the square root of the drifting rate. In order to obtain a comparable shift with high frequency forcing alone, a much larger amplitude is required. In contrast, for low frequency forcing, it is possible to obtain a larger advance than in the case of high frequency forcing. Since white noise forcing includes both high and low frequencies, the conditions for advancing the tipping point as indicated in the analysis of low frequency forcing are captured in the noisy forcing.

There are a number of questions remaining concerning the influence of oscillatory and noisy forcing on a system with a slowly drifting bifurcation. Here and in [14, 16] the case of additive forcing has been considered, but in general the oscillatory and noisy forcing can be multiplicative or parametric, as can be seen explicitly in the model considered in [11] without averaging over seasonal periodicity. In addition, the combination of noisy and oscillatory forcing should be of interest, as they appear together in applications. For example, for low frequency oscillations, we see that the location of the tipping point depends on the phase, and we would expect that the noise causes phase shifts. The question then remains when and if stochastic phase shifts, in combination with periodic forcing, play a significant role in the tipping location. A related area is the phenomenon of rate-induced tipping, where exceeding a critical drifting rate can result in early tipping [6]. The effect of noisy or oscillatory forcing on these types of transitions has not been analyzed.

The shift of the tipping point observed for different types of oscillations indicates that we must consider their effect on transitions via a saddle node bifurcation. For example, a common underlying structure for a hysteresis loop consists of two branches for stable states with a bistability region and loss of stability via saddle node bifurcations. If oscillations are included that advance the tipping points, the size of the hysteresis loop can be reduced, or the hysteresis can be removed completely.

More generally in a slow-fast system where the slow variable plays the role of a bifurcation parameter for the rest of the system, any oscillatory forcing can change the time to transition when a saddle node bifurcation is embedded in the system's structure. Complex phenomena

such as bursting dynamics or mixed-mode oscillations typically appear in slow-fast systems and involve combinations of transitions via different types of bifurcation with a slow variable viewed as a bifurcation parameter. For phenomena of this type in which a saddle node bifurcation is present, the results in this paper can quantify the influence of oscillations on the length of the intervals where steady states are attracting. In addition to the saddle node bifurcation considered here, there are other types of bifurcations that are potentially sensitive to combinations of slowly drifting parameters and oscillatory and noisy forcings. This sensitivity has been studied in other contexts, including different types of bifurcations [16, 18, 38], although not necessarily from the point of view of considering competitive or combined effects of both oscillations and noise on transitions or bifurcations.

Appendix A. The higher order analysis for $\mu = 0$ and $\Omega \gg 1$. We continue the asymptotic analysis in section 3.1 after (11) for $O(\Omega^{-2})$ and $O(\Omega^{-3})$, yielding

$$O(\Omega^{-2}) : x_{2T} + x_{1t} = -2x_0x_1, \Rightarrow x_{2T} = R_2(T,t) = -v_{1t} - 2x_0v_1 + 2Ax_0\cos(T), \tag{92}$$

$$O(\Omega^{-3}) : x_{3T} + x_{2t} = -x_1^2 - 2x_0x_2, \Rightarrow x_{3T} = R_3(T,t) = -x_{2t} - x_1^2 - 2x_0x_2. \tag{93}$$

By applying the solvability condition (9) to (92) and (93) and solving the resulting equations, we have

$$O(\Omega^{-2}) : v_{1t} = -2x_0v_1, \tag{94}$$

$$x_{2T} = 2Ax_0\cos(T), \ \Rightarrow x_2 = 2\sqrt{a}A\sin(T) + v_2(t), \tag{95}$$

$$O(\Omega^{-3}) : v_{2t} = -\frac{A^2}{2} - 2\sqrt{a}v_2. \tag{96}$$

The attracting solutions of (94) and (96) are their stable equilibria, which are $v_1 = 0$ and $v_2 = -\frac{A^2}{4\sqrt{a}}$. After substituting these equilibria and (11) and (95) into (6), we get (12) in section 3.1.

In order to find the local behavior of (1) with $\mu = 0$, we substitute $a = \Omega^{-2}b$ into (5) and get

$$x_T + \Omega^{-1}x_t = \Omega^{-3}b - \Omega^{-1}x^2 + \Omega^{-1}A\sin(T). \tag{97}$$

The contributions at each order are

$$O(\Omega^0) : \quad x_{0T} = 0, \ \Rightarrow \ x_0 = x_0(t), \tag{98}$$

$$O(\Omega^{-1}) : \quad x_{1T} + x_{0t} = -x_0^2 + A\sin(T), \ \Rightarrow x_{1T} = -x_{0t} - x_0^2 + A\sin(T), \tag{99}$$

$$O(\Omega^{-2}) : \quad x_{2T} + x_{1t} = 0, \ \Rightarrow x_{2T} = -x_{1t}, \tag{100}$$

$$O(\Omega^{-3}) : \quad x_{3T} + x_{2t} = b - x_1^2, \ \Rightarrow x_{3T} = -x_{2t} + b - x_1^2. \tag{101}$$

Substituting (98) into (99), applying the solvability condition (9), and solving the resulting equations, we have

$$x_{0t} = -x_0^2, \ \Rightarrow \ x_0 = 0, \tag{102}$$

$$x_{1T} = A\sin(T), \ \Rightarrow \ x_1 = -A\cos(T) + v_1(t). \tag{103}$$

Substituting (103) into (100) and applying the solvability condition (9), we have

$$v_{1t} = 0, \ \Rightarrow \ v_1 = d, \ \Rightarrow \ x_{2T} = 0, \ \Rightarrow \ x_2 = x_2(t), \tag{104}$$

where d is constant and needs to be determined. Substituting (103) and (104) into (101) and applying the solvability condition (9), we have

$$x_{2t} = b - \frac{A^2}{2} - d^2, \ \Rightarrow d^2 = b - \frac{A^2}{2}, \tag{105}$$

which provides the equilibrium solution of x_2. If $b - \frac{A^2}{2} < 0$, x_{2t} is always negative and there is no attracting solution.

By substituting (102), (103), (104), and (105) into (6), we have the leading order approximation (13) in section 3.1.

Appendix B. The asymptotic approximation of the solution for $0 < \mu \ll 1$ and $\Omega \gg 1$ in the outer region. We substitute (15) into (14), yielding

$$\begin{aligned} O(1) &: x_{0T} = 0, \ \Rightarrow \ x_0 = x_0(\tau), \\ O(\mu^\lambda) &: x_{1T} = a - x_0^2 + A\sin(T). \end{aligned} \tag{106}$$

Applying the solvability condition (9) of (106) and solving the resulting equations yields

$$\begin{aligned} x_0^2 = a, \quad &\Rightarrow \quad x_0 = \sqrt{a}, \\ x_{1T} = A\sin(T), \quad &\Rightarrow \quad x_1 = -A\cos(T) + v_1(\tau). \end{aligned}$$

The higher order contributions of (14) depend on the value of λ. The two cases are as follows:

$$\text{for } 0 < \lambda \le 1, \qquad O(\mu^{2\lambda}) : \mu^{1-\lambda} x_{0\tau} + x_{2T} = -2x_0 x_1; \tag{107}$$

$$\text{for } \lambda > 1, \qquad O(\mu^{1+\lambda}) : x_{0\tau} + x_{2T} = \mu^{\lambda-1} \cdot (-2x_0 x_1). \tag{108}$$

In either case, we substitute $x_0 = \sqrt{a}$ into (107) or (108) and apply the solvability condition (9), to get

$$x_{0\tau} = \mu^{\lambda-1}(-2x_0 v_1) \ \Rightarrow \ v_1 = \mu^{1-\lambda} \cdot \frac{1}{4a}.$$

Then the asymptotic approximation of the attracting solution is the result (16) of section 3.2.

Appendix C. The local approximation for $\Omega \ll 1$, near a_m. Writing (26) in terms of the local variables η, ξ, and A_m by (33), we have

$$-\mu\xi_\eta = a_m[1 - \cos(c\mu\eta)] + \mu\eta - \frac{1}{c}\sin(c\mu\eta) - \mu\frac{A_1 a_m}{A_m}\cos(c\mu\eta) - \mu\frac{A_1}{cA_m}\sin(c\mu\eta) - \mu^2\xi^2. \tag{109}$$

Substituting the expansion $\xi \sim \xi_0 + \mu\xi_1 + \mu^2\xi_2 + \cdots$ into (109) yields

$$\begin{aligned} O(\mu) &: -\xi_{0\eta} = -\frac{A_1 a_m}{A_m} \ \Rightarrow \ \xi_0 = \frac{A_1 a_m}{A_m}\eta + c_0, \\ O(\mu^2) &: -\xi_{1\eta} = \frac{1}{2}a_m c^2 \eta^2 - \frac{A_1}{A_m}\eta - \xi_0^2 \end{aligned} \tag{110}$$

$$\Rightarrow \xi_1 = -\left(\frac{1}{2}c^2 a_m - \frac{A_1^2 a_m^2}{A_m^2}\right)\frac{\eta^3}{3} + \frac{A_1}{A_m}(1+2c_0 a_m)\frac{\eta^2}{2} + c_0^2\eta + c_1, \tag{111}$$

which provides the local approximation (36). We find c_0 by writing (36) in terms of x and an intermediate scaled variable $a - a_m = \mathcal{K}\mu^q$ for $q < 1$ and $\mathcal{K}$ an $O(1)$ positive constant, to get

$$x = \frac{A_1 a_m}{A_m}\cdot\mathcal{K}\mu^q + \mu c_0 - \left(\frac{1}{2}c^2 a_m - \frac{A_1^2 a_m^2}{A_m^2}\right)\frac{\mathcal{K}^3\mu^{3q-1}}{3} + \frac{A_1}{2A_m}(1+2c_0 a_m)\mathcal{K}^2\mu^{2q} + \mu^{1+q}c^2\mathcal{K} + \mu^2 c_1 + \cdots \tag{112}$$

and match (112) with the Taylor expansion of the outer approximation (27) around a_m written in terms of $\mathcal{K}$:

$$x = \mu^q \cdot \sqrt{\frac{c^2 a_m}{2}}\mathcal{K} + \mu^{1-q}\cdot\frac{1}{2\mathcal{K}}\left(1 - \frac{A_1 a_m}{A_m c\sqrt{2a_m}}\right) + O(\mu^{2q}, \mu^{2-3q}). \tag{113}$$

We take $\frac{1}{3} < q < \frac{1}{2}$ so that the outer approximation (113) is valid. By matching the lower order terms in (112) and (113), we find c_0 in the form of $c_0 = -\frac{1}{2a_m} + C_1 + C_2$. This form is convenient for comparing with the ξ-intercept $-1/(2a_m)$ of the concavity threshold (35), reducing this comparison to determining the sign of $C_1 + C_2$, given by

$$C_1 = \mu^{-q}\frac{A_m}{\mathcal{K}a_m A_1}\left(\sqrt{\frac{c^2 a_m}{2}} - \frac{A_1 a_m}{A_m}\right) + \mu^{1-3q}\frac{A_m}{2\mathcal{K}^3 a_m A_1}\left(1 - \frac{A_1 a_m}{A_m c\sqrt{2a_m}}\right),$$
$$C_2 = \mu^{q-1}\frac{A_m}{3a_m A_1}\left(\frac{1}{2}c^2 a_m - \frac{A_1^2 a_m^2}{A_m^2}\right).$$

We find c_0 for $A > A_m$ only, since $A_c > A_m$ by the definition of A_m and a_m. If $\frac{A_1 a_m}{A_m} < \frac{c^2 A_m}{2A_1}$ and $A > A_m$, both C_1 and C_2 are positive and $c_0 > -\frac{1}{2a_m}$. Then the local trajectory (36) is in the concave-up region as assumed for $A_c > A > A_m$ and $a \le a_m$ ($\eta \le 0$). If $\frac{A_1 a_m}{A_m} > \frac{c^2 A_m}{2A_1}$, both C_1 and C_2 are negative. In that case the local trajectory (36) is in the concave-down region for $a \le a_m$ ($\eta \le 0$), resulting in tipping near $a = a_m$.

Appendix D. The local approximation for w in the ML model with $\Omega \gg 1$. The equations for the corrections z_1 and W_1 are

$$z_{1T} \sim -\mu^{1/3}z_{0s} + \left[b + (h_0^0 + h_1^0(\mathcal{X}+z_0) + h_2^0(\mathcal{X}+z_0)^2) - g_K(\mathcal{X}+z_0+\mathcal{D})W_0\right], \tag{114}$$

$$W_{1T} = -\mu^{1/3}W_{0s} + \left(\kappa(0) + \kappa'(0)(\mathcal{X}+z_0) + \frac{\kappa''(0)}{2}(\mathcal{X}+z_0)^2\right)$$
$$\cdot\left(w_\infty(0) + w'_\infty(0)(\mathcal{X}+z_0) + \frac{w''_\infty(0)}{2}(\mathcal{X}+z_0)^2 - W_0\right), \tag{115}$$

where we have kept linear and quadratic terms in $\mathcal{X}$ and z_0, analogous to (20). We apply the solvability condition as in (56), yielding for W_0

$$W_0 = \frac{\lim_{L\to\infty} L^{-1}\int_0^L(\kappa(0)+\kappa'(0)(\mathcal{X}+z_0)+\kappa''(0)(\mathcal{X}+z_0)^2/2)(w_\infty(0)+w'_\infty(0)(\mathcal{X}+z_0)+w''_\infty(0)(\mathcal{X}+z_0)^2/2)\,dT}{\lim_{L\to\infty} L^{-1}\int_0^L(\kappa(0)+\kappa'(0)(\mathcal{X}+z_0)+\kappa''(0)(\mathcal{X}+z_0)^2/2)\,dT}$$

$$
\begin{aligned}
&\approx w_\infty(0) + W_{00} + W_{01} z_0 + W_{02} z_0^2, \\
W_{00} &= \frac{w'_\infty(0)\kappa'(0) + w''_\infty(0)\kappa(0)/2}{W_{0d}} \frac{A^2}{2\Omega^2} + O(A^4/\Omega^4), \\
W_{01} &= \frac{w'_\infty(0)\kappa(0)}{W_{0d}} - \frac{\kappa'(0) W_{00}}{W_{0d}} + O(A^2/\Omega^2), \\
W_{02} &= W_{00}\left(\frac{2\Omega^2}{A^2} - \frac{\kappa''(0)}{2W_{0d}} + \frac{2\kappa'(0)^2}{W_{0d}^2}\right) - \frac{w'_\infty(0)\kappa'(0)\kappa(0)}{W_{0d}^2} + O(A^2/\Omega^2), \\
W_{0d} &= \kappa(0) + \frac{A^2\kappa''(0)}{4\Omega^2},
\end{aligned}
\tag{116}
$$

where we have used a Taylor series about z_0 to obtain a second order polynomial in z_0 as an approximation for W_0. Substituting (116) in the equation for z_0 written in terms of the original time scale yields (61). We note that the main contributions in the equation for z_0, used to determine the shift in the tipping point, are the terms involving h_j^0 and $g_k w_\infty(0)$. The additional terms with coefficients involving the derivatives of w_∞ and A^2/Ω^2 give small corrections, since these coefficients are small relative to g_K and the terms with h_j^0.

REFERENCES

[1] T.M. Lenton, H. Held, E. Kriegler, J.W. Hall, W. Lucht, S. Rahmstorf, and H.J. Schellnhuber, *Tipping elements in the earth's climate system*, Proc. Natl. Acad. Sci. USA, 105 (2008), pp. 1786–1793.

[2] A. Sutera, *On stochastic perturbation and long-term climate behaviour*, Quart. J. Roy. Meteor. Soc., 107 (1981), pp. 137–151.

[3] V. Guttal and C. Jayaprakash, *Changing skewness: An early warning signal of regime shifts in ecosystems*, Ecol. Lett., 11 (2008), pp. 450–460.

[4] C. Meisel and C. Kuehn, *Scaling effects and spatio-temporal multilevel dynamics in epileptic seizures*, PLos ONE, 7 (2012), e30371.

[5] L. Dai, D. Vorselen, K.S. Korolev, and J. Gore, *Generic indicators for loss of resilience before a tipping point leading to population collapse*, Science, 336 (2012), pp. 1175–1177.

[6] P. Ashwin, S. Wieczorek, R. Vitolo, and P. Cox, *Tipping points in open systems: Bifurcation, noise-induced and rate-dependent examples in the climate system*, Philos. Trans. R. Soc. Ser. A, 370 (2012), pp. 1166–1184.

[7] P. Mandel and T. Erneux, *The slow passage through a steady bifurcation: Delay and memory effects*, J. Stat. Phys., 48 (1987), pp. 1059–1070.

[8] S.M. Baer, T. Erneux, and J. Rinzel, *The slow passage through a Hopf bifurcation: Delay, memory effects, and resonance*, SIAM J. Appl. Math., 49 (1989), pp. 55–71.

[9] R. Haberman, *Slowly varying jump and transition phenomena associated with algebraic bifurcation problems*, SIAM J. Appl. Math., 37 (1979), pp. 69–106.

[10] K. Fraedrich, *Structural and stochastic analysis of a zero-dimensional climate system*, Quart. J. Roy. Meteor. Soc., 104 (1978), pp. 461–474.

[11] I. Eisenman and J.S. Wettlaufer, *Nonlinear threshold behavior during the loss of Arctic sea ice*, Proc. Natl. Acad. Sci. USA, 106 (2009), pp. 28–32.

[12] D.S. Abbot, M. Silber, and R.T. Pierrehumbert, *Bifurcations leading to summer Arctic sea ice loss*, J. Geophys. Res., 116 (2011), D19120.

[13] W.J. Merryfield, M.M. Holland, and A.H. Monahan, *Multiple equilibria and abrupt transition in Arctic summer sea ice extent*, in Arctic Sea Ice Decline: Observations, Projections, Mechanisms,

and Implications, C.M. Bitz, E.T. Deweaver, and L.B. Tremblay, eds., American Geophysical Union, Washington, DC, 2008, pp. 151–174.
[14] J. Sieber and J.M. Thompson, *Nonlinear softening as a predictive precursor to climate tipping*, Philos. Trans. Roy. Soc. Ser. A Math. Phys. Eng. Sci., 370 (2012), pp. 1205–1227.
[15] J.M.T. Thompson and J. Sieber, *Climate tipping as a noisy bifurcation: A predictive technique*, IMA J. Appl. Math., 76 (2011), pp. 27–46.
[16] N. Berglund and B. Gentz, *Stochastic dynamic bifurcations and excitability*, in Stochastic Methods in Neuroscience, C. Laing and G.J. Lord, eds., Oxford University Press, Oxford, UK, 2010, pp. 65–93.
[17] J. Zhu and R. Kuske, *Multiple Scale WKB-Type Approximations for Probability Densities in Stochastic Delayed Saddle Node Bifurcations*, preprint.
[18] R. Kuske, *Probability densities for noisy delay bifurcations*, J. Stat. Phys., 96 (1999), pp. 797–816.
[19] V. Dakos, M. Scheffer, E.H. van Nes, V. Brovkin, V. Petoukhov, and H. Held, *Slowing down as an early warning signal for abrupt climate change*, Proc. Natl. Acad. Sci. USA, 105 (2008), pp. 14308–14312.
[20] M. Scheffer, S.R. Carpenter, T.M. Lenton, J. Bascopmpte, W. Brock, V. Dakos, J. van de Koppel, I.A. van de Leemput, S.A. Levin, E.H. van Nes, M. Pascual, and J. Vandermeer, *Anticipating critical transitions*, Science, 338 (2012), pp. 344–348.
[21] K.K. Tung and J. Zhou, *Using data to attribute episodes of warming and cooling in instrumental records*, Proc. Natl. Acad. Sci. USA, 110 (2013), pp. 2058–2063.
[22] C.M. Bender and S.A. Orszag, *Advanced Mathematical Methods for Scientists and Engineers*, McGraw-Hill, New York, 1978, section 11.3.
[23] J. Kevorkian and J.D. Cole, *Perturbation Methods in Applied Mathematics*, Appl. Math. Sci. 34, Springer, New York, 1981.
[24] J. Kevorkian and J.D. Cole, *Multiple Scale and Singular Perturbation Methods*, Appl. Math. Sci. 114, Springer, New York, 1996.
[25] S.H. Strogatz, *Nonlinear Dynamics and Chaos*, Addison-Wesley, Reading, MA, 1994.
[26] T. Erneux and J.-P. Laplante, *Jump transition due to a time-dependent bifurcation parameter in the bistable ioadate-arsenous acid reaction*, J. Chem. Phys., 90 (1989), pp. 6129–6134.
[27] P. Jung, G. Gray, and R. Roy, *Scaling law for dynamical hysteresis*, Phys. Rev. Lett., 65 (1990), pp. 1873–1876.
[28] A. Hohl, H.J.C. van der Linden, R. Roy, G. Goldstein, F. Broner, and S.H. Strogatz, *Scaling laws for dynamical hysteresis in a multidimensional laser system*, Phys. Rev. Lett., 74 (1995), pp. 2220–2223.
[29] G.A. Maykut and N. Untersteiner, *Some results from a time-dependent thermodynamic model of sea ice*, J. Geophys. Res., 76 (1971), pp. 1550–1575.
[30] K.C. Armour, I. Eisenman, E. Blanchard-Wrigglesworth, K.E. McCusker, and C.M. Bitz, *The reversibility of sea ice loss in a state-of-the-art climate model*, Geophys. Res. Lett., 38 (2011), L16705.
[31] I. Eisenman, *Factors controlling the bifurcation structure of sea ice retreat*, J. Geophys. Res., 117 (2012), D01111.
[32] C. Morris and H. Lecar, *Voltage oscillations in the barnacle giant muscle*, Biophys. J., 35 (1981), pp. 193–213.
[33] *Morris-Lecar model*, Scholarpedia, http://www.scholarpedia.org/article/Morris-Lecar_model.
[34] N. Yu, Y. Li, and R. Kuske, *A computational study of spike time reliability in two types of threshold dynamics*, J. Math. Neurosci., 3 (2013), 11.
[35] *Morris–Lecar model*, Wikipedia, http://en.wikipedia.org/wiki/Morris-Lecar_model.
[36] S. Lee, *Study on the onset bifurcations of a Morris-Lecar neuron under a periodic current*, J. Korean Phys. Soc., 50 (2007), pp. 346–350.
[37] S. Lee, *Bifurcation analysis of a mode-locking structure in a strongly forced Morris-Lecar neuron*, J. Korean Phys. Soc., 52 (2008), pp. 11–16.
[38] P. Borowksi and R. Kuske, *Characterizing noisy mixed mode oscillations in neuronal models*, Chaos, 20 (2010), 043117.